


Cite this: *RSC Adv.*, 2024, 14, 7468

# From bench to industry, the application of all-inorganic solid base materials in traditional heterogeneous catalysis: a mini review

Zhixuan Zuo,<sup>†</sup> Yuchen Sha,<sup>†</sup> Peng Wang<sup>ID\*</sup> and Zhijian Da

Acids and bases generally occur in pairs as concepts, and a large number of catalytic reactions can be considered as interactions between acids and bases. Many chemical reactions are a combination of acid-catalyzed processes and base-catalyzed processes, and thus it is particularly important to study and explain the mechanisms of acid–base synergy or acid–base interactions. However, compared to the in-depth research on acid catalysts, there is a lack of research on solid bases. In addition to the application of basic materials to non-petroleum processes, recent studies have also applied basic materials to the catalytic cracking reaction process of heavy oils, providing new ideas for the processing of heavy oils. The formation of carbanions with the contribution of basicity is a critical stage in many fine chemical reactions, as well as in the hydrocarbon cracking reactions promoted by a base. Thus, herein, we summarize the research progress on the main types of all-inorganic solid base catalysts, including the types of catalysts used in non-petroleum processes and petroleum processes, their preparation, the properties of their basic sites, and their structure–performance correlation in the reactions. Also, we provide an outlook on the future research directions of all-inorganic solid base materials.

Received 13th January 2024  
Accepted 15th February 2024

DOI: 10.1039/d4ra00335g

rsc.li/rsc-advances

## 1 Introduction

Nowadays, environmental protection has become one of the most pivotal global issues. In terms of the chemical industry, the requirements of generating less pollutants and lower carbon emissions are becoming much more stringent, driving

the further development of new processes and catalysts. Heterogeneous catalysis is the most critical process in the modern chemical industry.<sup>1,2</sup> Generally, heterogeneous catalysts can be categorized into two parts, namely, solid acid catalyst and solid base catalyst. During the past few decades, both the fundamental research and industrial application of solid acid catalysts have been increasing rapidly and extensively with the booming petrochemical industry. In contrast, solid base materials have attracted less attention as catalysts

Sinopec Research Institute of Petroleum Processing CO., Ltd, No. 18 Xueyuan Road, Haidian District, Beijing 100083, P.R. China. E-mail: wangpeng.ripp@sinopec.com; Tel: +86-10-82368650

<sup>†</sup> These two authors contribute equally to this work.


Zhixuan Zuo

Zhixuan Zuo obtained his ME Degree in Chemical Engineering from the China University of Petroleum (Beijing) in 2021. He is currently working toward a PhD Degree under the direction of Prof. Zhijian Da in Chemical Technology with the Sinopec Research Institute of Petroleum Processing CO., LTD. His main research interests are the preparation and characterization of solid base catalysts, reaction mechanisms in hydrocarbon cracking, and applications in petrochemicals.



Yuchen Sha

Dr Yuchen Sha is an Associate Scientist at the Sinopec Research Institute of Petroleum Processing CO., LTD. He received his PhD from Wuhan University in 2021 working on the synthesis of nanocrystals and their application in organic synthesis. His current research interest mainly focuses on the development of the advanced catalysts for fluid catalytic cracking and deep catalytic cracking processes.



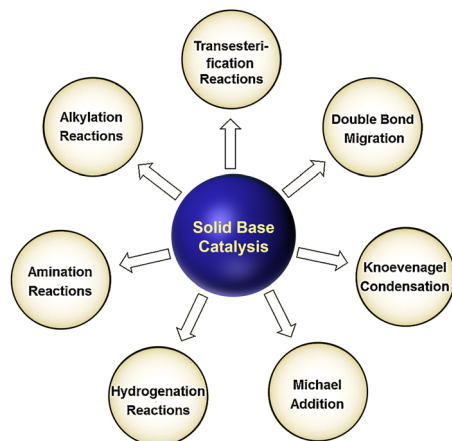


Fig. 1 Some typical fine chemical reactions catalyzed by solid bases.<sup>6</sup> Reprinted with permission from ref. 6. Copyright © 2015, The Royal Society of Chemistry.

probably due to their complicated preparation, propensity to be contaminated, etc.

According to the Brønsted acid–base theory and Lewis acid–base theory, it is well-accepted that a solid base material can serve as a catalyst either by abstracting a proton from the reactant or donating electron pairs to the reactant.<sup>3,4</sup> The history of solid base catalysts can be traced back to 1958 when Pines and co-workers showed that alumina-supported sodium metal could work as an effective catalyst for the double bond isomerization of alkenes.<sup>5</sup> Previously, most of the applications of solid bases in catalytic processes were concentrated in the catalysis and synthesis of fine chemicals in non-refinery fields such as olefin and alkyne isomerization, aldol condensation, and Henry reaction, as shown in Fig. 1.<sup>6</sup>

In recent years, several studies on the use of solid base catalysts for hydrocarbon catalytic cracking in oil refining have emerged; studies on catalytic cracking using solid base

materials have also emerged recently due to the high residual carbon problems resulting from the increasing heaviness of oil around the world and the use of heterogeneous catalysts prepared with solid base materials that have better resistance to carbon deposition in petroleum processes than acid catalysts<sup>7–9</sup>

Solid base materials are used in a wide range of applications; however, the present preparation process of solidbase materials, especially solid superbases, is more complicated and expensive compared with that of solid acid catalysts. Generally, as-prepared solid base materials possess a small specific surface area, poor structural strength, and weak hydrothermal stability. Moreover, both CO<sub>2</sub> and H<sub>2</sub>O in the air are easily adsorbed on the active sites of solid bases, leading to their undesirable passivation, thus reducing the catalytic activity of the catalyst.<sup>3,4,10,11</sup>

To date, there are several excellent reviews summarizing the application of solid bases in refining or non-refining fields.<sup>1,3,12–20</sup> According to the analysis of the references in the literature, to date, the catalytic mechanism for base-catalyzed processes has not been explained in detail, and the structure–activity relationships between the physical and chemical properties of these catalysts and reactions have not been well established. Therefore, a systematic study on the mechanism of solid base catalysis is required to establish the structure–activity relationships between catalytic properties and physical and chemical properties of catalysts, which will be more helpful for the in-depth understanding and application improvement of solid bases. However, to date, a comprehensive description of the application of solid base catalysts in both fields has not been reported, and thus, herein, we summarize the general categories of all-inorganic solid base catalytic materials first, and then review the preparation, properties, and applications of metal oxide and zeolite-based solid base materials in non-refinery and refinery fields, which have been reported in numerous studies, to provide some guidance for the follow-up preparation and studies on improving these materials.



Peng Wang

Dr Peng Wang is a Scientist at the Sinopec Research Institute of Petroleum Processing CO., LTD. She received her PhD from the Sinopec Research Institute of Petroleum Processing CO., Ltd in 2006 working on the development of catalysts for fluid catalytic cracking. She is a senior expert on R&D of catalytic cracking catalysts and zeolite. She has rich experience in this field and developed more than 10 commercialized cata-

lysts. Her number of authorized patents reached one hundred recently.



Zhijian Da

Dr Zhijian Da is a Senior Scientific and Technical Advisor and PhD supervisor at the Sinopec Research Institute of Petroleum Processing CO., LTD. He received his M.E and PhD degrees from the Sinopec Research Institute of Petroleum Processing CO., Ltd in 1988 and 1991, respectively. From 1996 to 1997, he undertook postdoctoral research at the CNRS and at the Organocatalytic Research Unit of the University of Poitiers. He

has been engaged in the research and development of molecular sieve catalytic materials, FCC catalyst preparation, and refining-related processes.



## 2 Categories of all-inorganic solid base catalysts

Different types of solid base catalysts and various basic sites generate different effects in multiple fine chemical processes and refining processes.<sup>13,21–23</sup> These solid base catalysts range from single-component oxides to complex-component oxides and even zeolites. The most accepted definitions of solid surface acids and bases by researchers are those proposed by Brønsted and Lewis, where a Brønsted base is defined as the opposite of a Brønsted acid, namely, a substance that can take protons from reactants; a Lewis base is an electron donor that gives electron pairs.<sup>24</sup> The type and strength of the base sites differ in catalytic reaction processes and results. Table 1 presents several types of commonly used all-inorganic solid base catalysts, which are grouped based on their composition and typical active components.<sup>3</sup>

## 3 Metal oxide solid bases

At present, the research on metal oxide solid bases generally focuses on alkali and alkaline earth metal oxides, which are the earliest and most deeply researched solid base materials, but in the early stage of their industrial application.<sup>4,25,26</sup> Recently, some commonly used methods for the preparation of metal oxide catalysts were summarized by Védrine.<sup>26</sup> In the case of simple oxides, their preparation is usually based on three main series of conventional preparation routes, *i.e.*, gas-phase polymerization, aqueous-phase precipitation, and hydrolytic or non-hydrolytic sol-gel processing. For mixed oxides, the most common technique is the co-precipitation method, where two metal salts are mixed in solution and precipitated at a given pH. Generally, supported oxide catalysts are prepared using ambient temperature, aqueous phase methods such as selective adsorption, impregnation and deposition-precipitation. Also, these methods are dominant on an industrial scale due to environmental and economic reasons. Further, their surface functionality can be adjusted by incorporating active sites in the walls of silica or depositing active substances on the inner surface of the materials to synthesize mesoporous silica-based materials with better physicochemical and textural properties and optimized catalytic properties.<sup>26,27</sup> Therefore, some important routes for the preparation of metal oxide solid bases are provided in the following, which also include rare earth oxides and other oxides, while other oxides mainly include loaded oxides and mixed oxides.

### 3.1 Alkaline earth metal oxides

**3.1.1 Intrinsic properties.** Several typical alkaline earth metal oxides such as MgO, CaO, SrO, and BaO have been used as solid base catalysts for a variety of reactions. Among them, magnesium oxide (MgO) is one of the most abundant elements on Earth and present in the form of rocks such as dolomite, silicate, and magnesite. Moreover, magnesium oxide is also present in seawater and produced mainly by the calcination of magnesite (MgCO<sub>3</sub>). Owing to the simplicity of both its preparation method and obtaining well-structured materials, MgO has attracted increasing attention compared to other alkaline earth metals. Among the above-mentioned four metal oxides, MgO and CaO are generally prepared *via* the calcination of Mg(OH)<sub>2</sub> and Ca(OH)<sub>2</sub>, respectively. In contrast, SrO and BaO cannot be prepared using a similar procedure given that the melting temperature of their corresponding hydroxide is lower, which easily causes severe sintering. Therefore, SrO and BaO are generally prepared *via* the calcination of their carbonates. However, the prepared oxides are inevitably be exposed to air, where CO<sub>2</sub> and H<sub>2</sub>O cover the base sites on the oxide surface, and thus the metal oxides must be calcined or treated by other methods to remove the surface impurities to restore their activity before loading and use.<sup>28,29</sup>

Nevertheless, another important drawback of the aforementioned metal oxide solid base catalysts compared with zeolites or other catalysts for industrialization is their lower specific surface area. For example, the typical commercial MgO only has a low specific surface area of around 20 m<sup>2</sup> g<sup>−1</sup>, resulting in a lower density of basic sites. Therefore, many studies have focused on enhancing its specific surface area. Recently, a route for the preparation of high specific surface area MgO from commercial MgO was reported, resulting in a specific surface area of up to 250 m<sup>2</sup> g<sup>−1</sup> and a basic site density of 2.5 mmol g<sup>−1</sup>, as determined by CO<sub>2</sub>-TPD.<sup>30</sup> However, due to the complexity of this method, it is expensive and difficult to apply. Ordonez *et al.* reported a new thermal treatment method to prepare MgO, as shown in Fig. 2(a). This novel method involved the processes of hydration and dehydration of periclase, which addresses the conflict between surface area enhancement and environmental benignity.<sup>31</sup> Various precursors and thermal treatments were investigated and the results indicated that the thermal treatment provided defects on the surface of magnesium oxide, which resulted in a large specific surface area (221 m<sup>2</sup> g<sup>−1</sup>) and a significant concentration of surface basic sites (1.2 mmol g<sup>−1</sup>). Also, the equilibrium adsorption isotherms at 0–6.7 kPa and 50 °C, as shown in

Table 1 Categories of widely used all-inorganic solid bases<sup>3</sup>

Type	Main active components
Intrinsic metal oxide	MgO, CaO, Al <sub>2</sub> O <sub>3</sub> , ZrO <sub>2</sub> , La <sub>2</sub> O <sub>3</sub> , Rb <sub>2</sub> O
Mixed oxide	SiO <sub>2</sub> –MgO, CaO–SiO <sub>2</sub> , MgO–Al <sub>2</sub> O <sub>3</sub>
Metal oxide loaded	Na <sub>2</sub> O/SiO <sub>2</sub> , MgO/SiO <sub>2</sub> , Cs <sub>2</sub> O/Zeolites
Alkali metal compound loaded	KF/Al <sub>2</sub> O <sub>3</sub> , K <sub>2</sub> CO <sub>3</sub> /Al <sub>2</sub> O <sub>3</sub> , KNO <sub>3</sub> /Al <sub>2</sub> O <sub>3</sub>
Alkali metal loaded	Na/Al <sub>2</sub> O <sub>3</sub> , K/Al <sub>2</sub> O <sub>3</sub> , K/MgO, Na/Zeolites
Metal ion-exchanged zeolite	K, Rb, Cs-exchanged X, Y zeolites



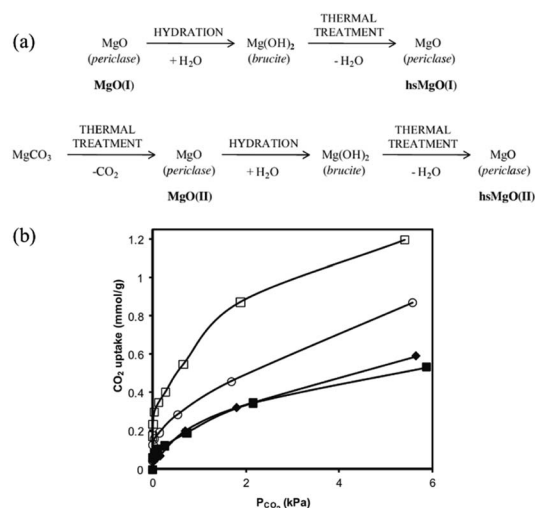


Fig. 2 (a) Proposed activation steps and notation (bold) used for the different MgO. (b)  $\text{CO}_2$  adsorption isotherms at 50 °C and 6.7 kPa, measured by microcalorimetry for  $\text{MgO(I)}$  (◆),  $\text{MgO(II)}$  (■),  $\text{hsMgO(I)}$  (□), and  $\text{hsMgO(II)}$  (○).<sup>31</sup> Reprinted with permission from ref. 31. Copyright © 2014, Elsevier.

Fig. 2(b), indicated the presence of combined chemisorption and physisorption mechanisms. The large improvement in  $\text{CO}_2$  uptake confirmed that a suitable pathway for modifying MgO was reasonably achieved.

In general, the basic strength of alkali metal and alkaline earth metal oxide catalysts increases as their atomic number increases, and the calcination temperature and the types of precursors also significantly affect the basic strength of alkali metals and alkaline earth metal oxides. Specifically, different calcining temperatures generally lead to different basic strengths, and the active sites of metal oxides can vary from one preparation process to another. Moreover, the activity and stability of the basic sites can be affected by the chemical environment of the active sites.<sup>32</sup> According to the above discussion, it can be seen that different treatment processes can regulate the base properties of metal oxide materials.

The active sites of metal oxides are mainly generated from the negatively charged lattice oxygen and hydroxyl groups formed by the adsorption of water on their surface. Anpo *et al.* discussed the different basic sites produced by various surface oxygen species on oxide materials and the electron paramagnetic resonance and photoluminescence techniques used for the characterization of paramagnetic ( $\text{O}^-$ ,  $\text{O}_2^-$ , and  $\text{O}_3^-$ ) and diamagnetic surface oxygen species ( $\text{O}_{2,\text{surf}}^-$ ), respectively.<sup>33</sup>

A classic example is shown in Fig. 3(a),<sup>34</sup> where the crystal structure of the conventional magnesium oxide is halite (cubic) in shape, with its crystal lattice tightly bonded in an octahedral shape and having a lattice constant of  $a = 4.212 \text{ \AA}$ . A schematic representation of the irregularities on the surface of MgO with impurities removed and the terminology presented by Chizallet *et al.* are shown in Fig. 3(b) and Table 2, respectively. The  $\text{O}^{2-}$  centers exist in different coordination numbers and at different positions and ion pairs with low coordination numbers are generally present at the corners of the MgO surface. Generally,

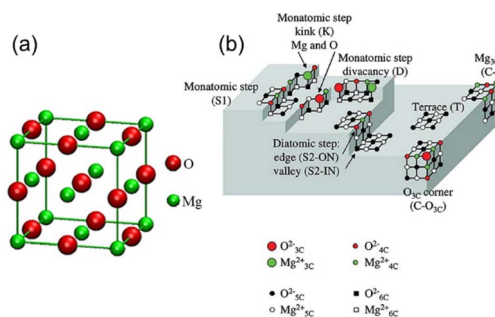


Fig. 3 (a) Crystal structure of MgO.<sup>34</sup> Reprinted with permission from ref. 34. Copyright © 2010, IOP. (b) Schematic representation of irregularities on the surface of MgO. The terminologies used are shown in Table 2.  $\text{Mg}_{3c}^{2+}$ : 3-coordinated  $\text{Mg}^{2+}$  on corners;  $\text{O}_{4c}^{2-}$ : 4-coordinated  $\text{O}^{2-}$  on edges.<sup>35</sup> Reprinted with permission from ref. 35. Copyright © 2011, Taylor & Francis.

these ion pairs possess the highest degree of unsaturation and the strongest basicity, while ion pairs with high coordination numbers are generally found on perfect crystalline surfaces or defect-free surface positions, which result in weaker basicity.<sup>35–39</sup> Among the ion pairs with different coordination numbers, the triple-coordinated Mg–O ion pairs have the strongest ability to adsorb carbon dioxide and water and have high relative activity, and thus the calcining temperature must be increased to expose these ion pairs. The ion pairs with different coordination numbers are exposed to the surface in sequence by a step-up temperature, while the active sites with different coordination numbers have different adsorption properties for water and carbon dioxide, and the triple-coordinated Mg–O ion pair has the highest desorption temperature due to the highest reactivity. However, the most reactive ion pair is prone to rearrangement and annihilation at higher temperatures due to its instability.<sup>37</sup> As the calcining temperature continues to increase, the highly unsaturated ion pairs will reach equilibrium between the process of generation and the process of disappearance of rearrangement, while the activity of MgO also reaches its maximum with an increase in the calcining temperature.<sup>35,37,39</sup>

**3.1.2 Performance in fine chemical catalysis.** The lower the coordination of the acid and base element pairs, the stronger

Table 2 Nature, label, and formula as used in Fig. 3 from ref. 35

Nature	Label	Formula
(100) plane	T	$\text{Mg}_{13}\text{O}_{14}\text{Mg}_{17}$
	T'	$\text{OMg}_5$
Monatomic step	S1	$\text{Mg}_{20}\text{O}_{14}\text{Mg}_{10}$
Diatomic step: edge	S2-ON	$\text{Mg}_{10}\text{O}_{10}\text{Mg}_{10}$
	S2-ON'	$\text{Mg}_{10}\text{O}_{16}\text{Mg}_{22}$
Diatomic step: valley	S2-IN	$\text{Mg}_{22}\text{O}_9$
Corner: $\text{O}_{3c}^{2-}$ -terminated	C- $\text{O}_{3c}$	$\text{Mg}_{13}\text{O}_{13}\text{Mg}_{12}$
Corner: $\text{Mg}_{3c}^{2+}$ -terminated	C- $\text{Mg}_{3c}$	$\text{Mg}_7\text{O}_9\text{Mg}_{10}$
Divacancy	D- $\text{Mg}_{3c}$ - $\text{O}_{3c}$	$\text{Mg}_9\text{O}_{10}\text{Mg}_{13}$
Kink: $\text{O}_{3c}^{2-}$ -terminated	K- $\text{O}_{3c}$	$\text{Mg}_{19}\text{O}_{13}\text{Mg}_9$
Kink: $\text{Mg}_{3c}^{2+}$ -terminated	K- $\text{Mg}_{3c}$	$\text{Mg}_{21}\text{O}_{14}\text{Mg}_{10}$



the proton capturing ability. Therefore, it is of great importance to study the surface of defective oxides in base-catalyzed reactions that require strong stabilization of deprotonated substances. Magnesium oxide pretreated at a moderate temperature of 750 K provided the maximum activity in the hept-1-ene isomerization reaction.<sup>40</sup> The transient formation of unstable magnesium oxide planes (1,1,1) or (1,1,0) was demonstrated by mixed experimental theoretical studies on carbon dioxide adsorption and by infrared spectroscopic analysis. The high basic strength of these unstable planes is now well recognized in the literature, as shown, for example, in the adsorption of carbon oxides.<sup>41</sup>

However, the strength of the basic sites required for solid base catalysis should be selected according to the change in the ease of extraction of protons from the reactants by the basic sites under the reaction conditions. For example, MgO requires a pretreatment temperature of 527 °C for catalytic 1-butene isomerization and 700 °C for CH<sub>4</sub>-D<sub>2</sub> exchange, and different pretreatment temperatures correspond to different base strengths.<sup>19</sup>

In the 1-butene isomerization reaction, the O<sup>2-</sup> active site on the surface of the solid base adsorbs hydrogen protons from the reactant molecules to form anionic intermediates, and the adjacent metal ions stabilize the anionic intermediates for subsequent reactions. The lattice oxygen O<sup>2-</sup> on the surface of the solid base CaO serves as a base center to adsorb the H on the isopropyl tertiary carbon atom of isopropylbenzene (IPB), and the interaction between H and the lattice oxygen weakens the C-H bond of the tertiary carbon atom and lowers the activation energy for radical formation, promoting the formation of radicals.<sup>42</sup> Another example is the alcohol-formaldehyde condensation of butyraldehyde, where the active center is not the surface hydroxyl group but the lattice oxygen O<sup>2-</sup>, which forms a stronger interaction with CO<sub>2</sub> and H<sub>2</sub>O.<sup>43</sup> In contrast, the relationship between the thermodynamic Brønsted basicity and kinetic basicity of magnesium oxide samples was investigated by comparing the results obtained from the deprotonation equilibrium of a protic molecule with the MBOH transformation as the model reaction. It was found that the hydroxylated surfaces are more reactive than the bare surfaces, despite their lower deprotonation capacity.<sup>44</sup>

Reaction path simulations of the nudged elastic band (NEB) method indicated that a bare Mg<sup>2+</sup>-O<sup>2-</sup> pair is available for MBOH adsorption and reaction occurs in the vicinity of the surface OH groups, which lowers the activation energy barrier.<sup>45</sup>

Although the OH groups do not interact directly with the MBOH reactant, they alter the basic reactivity of the bare Mg<sup>2+</sup>-O<sup>2-</sup> pairs in the vicinity where the adsorption and conversion of MBOH occur. Therefore, it can be seen that the same solid base catalyst has different active sites serving as base centers, and the active sites of the reaction are different for various reactions.

As consistently mentioned above, there are two other types of molecules that can be adsorbed, *i.e.*, CO<sub>2</sub> and H<sub>2</sub>O, which cannot be ignored. Generally, it is believed that they result in the passivation of the base center, but in some systems, this can be different, and the adsorption of both CO<sub>2</sub> and H<sub>2</sub>O molecules on the solid base also has different effects. For example, the

adsorption of CO<sub>2</sub> and H<sub>2</sub>O has almost no effect on the reaction between nitromethane and propionaldehyde because the reactants are more easily adsorbed at the base center than CO<sub>2</sub> and H<sub>2</sub>O, which inhibits them from poisoning the base sites, making it almost impossible to affect the catalyst activity.<sup>46</sup> Another example is the addition of a small amount of water in the hydroxyl aldehyde condensation reaction to improve the catalytic activity of the solid base to a certain extent, where researchers believe that the adsorption of water on the surface of the solid base increases the surface hydroxyl or O<sup>2-</sup> ions in the solid base, increasing the density of the base center.<sup>47</sup>

As discussed in the previous two sections, it can be seen that to gain strong basicity *via* certain oxides in certain reactions, the previous strategy was the modification of oxides with alkaline metals to create surface vacancies or defects, which suffer from instability under the catalytic conditions. Alternatively, single-component basic oxides (*e.g.*, magnesium oxide) are stable but have poor electron-withdrawing ability.

### 3.2 Rare earth oxides

**3.2.1 Intrinsic properties.** Rare earth oxides can be considered as both oxidant and strong bases. Usually, rare earth oxides are prepared by hydrolyzing aqueous nitrate solutions containing rare earths in ammonia, followed by the calcination of obtained hydroxides in air or high-temperature decomposition under vacuum. It is noteworthy that the stable forms of rare earth oxides obtained by this method are generally sesquioxide such as M<sub>2</sub>O<sub>3</sub>, while the stable states of Ce, Pr, and Tb are CeO<sub>2</sub>, Pr<sub>6</sub>O<sub>11</sub>, and Tb<sub>4</sub>O<sub>7</sub>, respectively. Simultaneously, rare earth oxides and alkaline metal oxides are similarly prone to strong interactions with CO<sub>2</sub> and H<sub>2</sub>O, resulting in structural changes when stored in air, making their storage and pre-treatment conditions for before use even more demanding.

**3.2.2 Performance in fine chemical catalysis.** The basic properties of many rare earth oxides are similar. In particular, La<sub>2</sub>O<sub>3</sub> was used for 1-butene isomerization, 1,3-butadiene hydrogenation, and CH<sub>4</sub>-D<sub>2</sub> exchange reactions, with all suitable pretreatment temperatures of 650 °C to provide the maximum activity.<sup>48–50</sup> IR studies indicate that this temperature is necessary to remove all the adsorbed CO<sub>2</sub> from the oxide surface to expose the strong base centers.<sup>51</sup>

In general, solid base catalysts promote the dehydrogenation of alcohols to aldehydes and ketones rather than the dehydration of alcohols in reactions, but rare earth oxides can show unique selectivity for alcohol dehydration reactions, *e.g.*, when the reaction product is mainly 1-butene (2-butanol dehydration product) in the case of using rare earth metal oxides such as ThO<sub>2</sub> as a solid base catalyst in the 2-butanol dehydration reaction.<sup>16,18,52,53</sup>

Rare earth oxides have not been widely used in base catalytic processes thus far because the mechanism of their base centers in the synthesis reactions of conventional fine chemicals as base catalysts is still unclear and poorly studied. However, researchers generally agree that the base centers on rare-earth oxides have significant catalytic properties for hydrogenation processes, especially given that many rare-earth oxides have



strong ethylene hydrogenation ability at  $-78\text{ }^{\circ}\text{C}$ .<sup>19,54</sup> Simultaneously, given that rare earth oxides are mainly involved in the oxidative cracking process in oil treatment, the process inevitably generates  $\text{CO}_x$  (carbon oxygen compounds), which not only inhibits the production of low carbon olefins, but also tends to lead to the poisoning of base catalysts. Thus, the above-mentioned drawbacks also limit the research on the application of rare earth oxides in petroleum refining.

### 3.3 Other oxides

**3.3.1 Intrinsic properties.** Other oxides are mainly mixtures prepared by loading two metals or their oxides, generally with a basic active center and a corresponding carrier. The active center of these mixtures drive the reaction, and the carrier can be active, while the chemical environment provided by the carrier can largely affect the catalytic performance of these mixtures. Generally, mixed oxides are prepared by mixing and calcining one or more oxides such as  $\text{MgO}$ ,  $\text{CeO}_2$ , and  $\text{Al}_2\text{O}_3$ .

Presently, more studies on basic mixed oxides used in the field of fine chemicals are focused on mixed base metal oxides and magnesium-aluminum oxides prepared from calcined hydrotalcite. Generally, acidic oxides can be made significantly more acidic by mixing oxides, while unlike the results of acidic mixed oxides, the basicity of basic mixed oxides and their properties can usually be modified only to a limited extent by the addition of other component oxides. It has been found that mixing two oxides does not significantly improve their basicity. Noller *et al.* studied the basicity of  $\text{MgO-Al}_2\text{O}_3$  and  $\text{MgO-SiO}_2$  by XPS and IR characterization of their hydroxyl groups, and also explored their catalytic activity in reactions.<sup>55</sup> The results showed that the basicity of this mixed oxide is usually between the base strengths of the two oxides, and thus the basicity strength is considered to be consistent with Sanderson's average electronegativity theory, which can be used as a guidance for following research work.

The modification of the surface of solid bases and their basicity can be achieved not only by mixing two or more types of oxides but also by loading other components on the metal oxides or mixed oxides, which can change their basicity and surface properties to some extent. The presence of different metal ions in a solid base has a significant effect on its basicity, *e.g.*, the introduction of metal ions in  $\text{MgO}$ . As shown in Fig. 4(a), the density of its basic sites increases if the radius of the metal ions is slightly larger than that of  $\text{Mg}^{2+}$ , while the introduction of metal ions with a smaller radius than  $\text{Mg}^{2+}$  has no significant effect.<sup>56</sup> A metal ion with an excessively large radius may not be able to dope the lattice of  $\text{MgO}$ , and therefore the change in basicity is small. Alternatively, a metal ion with a too small radius cannot elongate the bond length of the  $\text{Mg-O}$  bond and change the crystal structure, and therefore cannot effectively modulate the basicity of the oxide. Only when the metal ion radius is slightly larger than that of  $\text{Mg}^{2+}$  is causes lattice distortion, resulting in the elongation of the  $\text{Mg-O}$  bond and the electron delocalization effect of the lattice oxygen. The addition of an alkali metal to  $\text{MgO}$  can produce strong basic sites, as shown in Fig. 4(b). When an alkali metal atom is

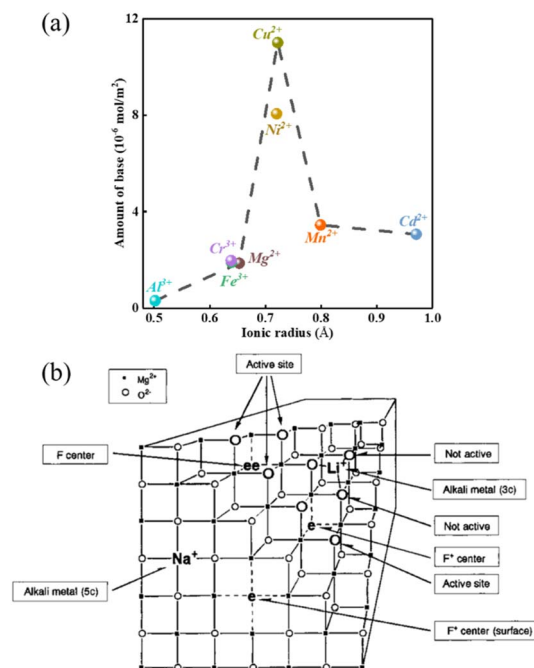


Fig. 4 (a) Relationship between the amount of base (density) on the surface of  $\text{MgO}$  and the radius of the doped metal ions.<sup>56</sup> Adapted with permission from ref. 56. Copyright © 2006, Oxford University Press. (b) Model for the super basic sites generated by the addition of alkali metal to  $\text{MgO}$ : 3-coordinated;  $\text{F}^+$  center: an electron attracted by a single oxygen vacancy; and F center: a pair of electrons attracted by a single oxygen vacancy.<sup>57</sup> Reprinted with permission from ref. 57. Copyright © 2000, the American Chemical Society.

adsorbed on the surface of  $\text{MgO}$  it releases an electron to the alkali metal ion, the released electron is attracted to a single oxygen vacancy on the subsurface to form an electron  $\text{F}^+$  center or F center of a pair of electrons, and the three  $\text{O}^{2-}$  ions present on the (111) crystal face adjacent to the  $\text{F}^+$  center or F center are the strongly basic sites (lattice  $\text{O}^{2-}$ ).<sup>57</sup> After loading Li on  $\text{MgO}$ , the excess cations lead to the formation of oxygen vacancies on the surface of  $\text{MgO}$ , and oxygen in the gas phase under a high temperature atmosphere reacts with the vacancies to produce  $\text{O}^{2-}$  and holes, which tend to be close to the  $\text{O}^{2-}$  near  $\text{Li}^+$ . Consequently, it generates a base center *via* the  $2\text{Li}^+\text{O}^{2-} + \text{X} + 1/2\text{O}_2 \rightarrow 2[\text{Li}^+\text{O}^-] + \text{O}^{2-}$  reaction to form the  $[\text{Li}^+\text{O}^-]$  center (X denotes an oxygen vacancy).<sup>35</sup> Similar to  $\text{MgO}$ , there are intrinsic defects in the transition metal oxide  $\text{TiO}_2$ , which can generate the corresponding oxygen vacancies to achieve the modulation of the other components introduced. The point defects such as oxygen vacancies and oxygen interstitials in  $\text{TiO}_2$  tend to attract and capture electrons to form electro-neutral complexes with the metal ions according to the theory of charge equilibrium and can be largely classified into the electron centers (F) and the electron vacancy centers ( $\text{V}_0$ ). The structure and formation process of various types of centers on  $\text{TiO}_2$  are shown in Fig. 5, in which there is no unpaired electron in the F center, there is an unpaired electron in the  $\text{F}^+$  center, and the two electrons in the F center tend to occupy the metal ions to form an  $\text{F}^{++}$  center with a positive charge.<sup>58</sup>



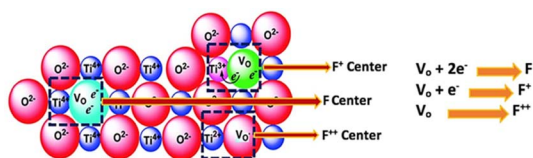


Fig. 5 Schematic illustration and description of various F centers formed in  $\text{TiO}_2$ . F center: four  $\text{Ti}^{4+}$  in the neighborhood with no unpaired electrons and  $\text{F}^+$  center:  $\text{Ti}_{\text{lattice}}^{3+}$  with an unpaired electron.<sup>58</sup> Reprinted with permission from ref. 58. Copyright © 2018, MDPI.

It is well known that catalytic reactions proceed at the defect sites in these oxide catalysts, *e.g.*, the basic sites generated from metal oxide vacancies of lattice oxygen  $\text{O}^{2-}$  or  $\text{O}^-$ , a monotonic relationship does not always exist between the catalytic performance and the concentration of oxygen vacancies, lattice distortions, and defect-produced Lewis bases.<sup>59–62</sup> In a pure oxide, the oxygen ions or vacancies usually have a high symmetric coordination with the cations. In recent years, researchers have paid more attention to the chemical environment of oxygen vacancies and have proposed “asymmetric oxygen vacancy sites,” which denote the asymmetric coordination of oxygen vacancies with cations, allowing oxygen to move more freely. The review article by Yu *et al.* well explained the “asymmetric oxygen vacancy site” and showed that the strength of cations of different sizes, electronic structures, oxidation states, and relatively stable coordination numbers can be adjusted to suit different chemical reactions, with the aim of equilibrating the adsorption and desorption of oxygen species.<sup>63</sup> For example, in the fluorite-type bulk structure of  $\text{CeO}_2$ , a simple way to break the oxygen/vacancy symmetry is to replace one of the cerium cations to form the asymmetric site  $\text{M}-\square(-\text{Ce})_3$  or  $\text{M}-\square(-\text{Ce})_3$ , where  $\square$  stands for the oxygen vacancy, as shown in Fig. 6(a). These  $\text{M}_1-\text{O}-\text{M}_2$  or  $\text{M}_1-\square-\text{M}_2$  sites coordinated to different cations can be denoted as “asymmetric oxygen vacancies” and the alternate formation of  $\text{M}_1-\text{O}-\text{M}_2$  and  $\text{M}_1-\square-\text{M}_2$  can serve as active sites.<sup>64,65</sup>

For example, the dispersed metal atoms on the surface of SACs are usually isolated catalytically active sites, but the reaction may take place on surrounding atoms such as oxygen in the substrate and active asymmetric oxygen vacancies in these

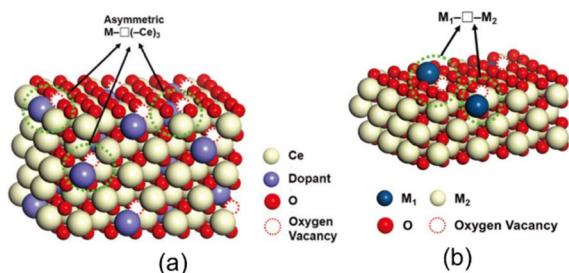


Fig. 6 (a) Asymmetric oxygen vacancy sites of  $\text{M}-\square(-\text{Ce})_3$  in doped ceria. (b) Asymmetric oxygen vacancy sites on the surface of SACs.<sup>63</sup> Reprinted with permission from ref. 63. Copyright © 2019, Wiley.

materials, as shown in Fig. 6(b). Nie *et al.* reported that the steam treatment of atomically dispersed  $\text{Pt}^{2+}/\text{CeO}_2$  catalysts can effectively create active surface lattice oxygen, which was produced by filling the surface oxygen vacancies ( $\text{Pt}-\square-\text{Ce}$ ) derived from the substitution of  $\text{Pt}^{2+}$  for  $\text{Ce}^{4+}$ .<sup>66</sup> Unlike other materials, almost all the platinum atoms in the above-mentioned materials are located on the oxide surface and each platinum atom activates two or more surrounding oxygen atoms.

**3.3.2 Performance in fine chemical catalysis.** Numerous solid base catalysts possess lattice oxygens, which serve as the active sites in reactions. Thus, lattice oxygens are considered to be highly pivotal active sites in most solid base materials based on metal oxides utilized for fine chemistry investigations, and a great deal of work focused on modulating the properties of lattice oxygens.

The selective oxidation of alcohol or dehydrogenation of alcohol to produce aldehyde also showed a demand for the use of base catalysts, where the base sites may be employed to remove H atoms from hydroxyl group and  $\alpha$ -carbon.<sup>67–69</sup> The first step in the selective oxidation of alcohols to produce the  $\eta^1$  (O)-configuration ( $\text{M}-\text{O}-\text{C}$ ) requires either a weakly acidic site or a strongly basic site for the O–H bond to break rather than the C–O bond, which leads to dehydration.<sup>70</sup> If the  $\eta^2$  (C, O)-configuration is formed, the weak basicity promotes  $\pi^*$ -bond interactions, and the active site with fewer electrons will be favorable for coordination by the lone pair of electrons of the O atoms, thus reducing the stability of the C–O bond.<sup>2</sup>

More recently, Cho *et al.* investigated the effects of a Ca-promoter on the catalytic activity of MgO given that they observed very different catalytic activities of MgO in the oxidative coupling of methane (OCM) resulting from the company that supplied the precursors.<sup>71</sup> The shift in the base properties of the surface lattice oxygen on the catalyst, as determined by  $\text{CO}_2$ -TPD and shown in Fig. 7(a), indicated that MA99 (99% Mg with 1% Ca, mole fraction) contained the largest amounts of lattice oxygen with weak and medium basicity, while MA0 (100% Ca, mole fraction) contained the largest amount of lattice oxygen with strong basicity. Hence, the appropriate addition of Ca to the MgO catalyst would enrich the formation of oxygen vacancies and lattice oxygen with medium basicity, which facilitates the reaction of the adsorbed oxygen species and methane to produce the methyl radical, whereas lattice oxygen with strong basicity would be established by an excessive Ca content. The lattice oxygen with medium basicity facilitates the dehydrogenation of  $\text{C}_2\text{H}_6$  to  $\text{C}_2\text{H}_4$ . On the contrary, lattice oxygen with strong basicity acts as a strong oxidant for the production of  $\text{CO}_2$  from various hydrocarbons. Due to the above-mentioned information between the catalytic activity and the properties, they proposed a process for the oxidative coupling of methane by surface oxygen species, as shown in Fig. 7(b).<sup>71</sup>

To enhance the basic strength of oxide-based solid base catalysts, Yang *et al.* developed  $\text{Ga}_4\text{B}_2\text{O}_9$  and evaluated its performance in reactions for the synthesis of  $\alpha$ -aminonitriles (Strecker reaction) and the selective conversion of n-propanol. It exhibited strong Lewis basicity, and further its activity was





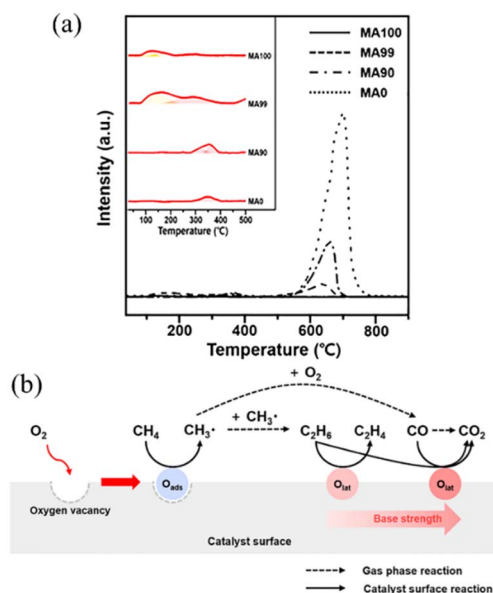


Fig. 7 (a) CO<sub>2</sub>-TPD profiles of catalysts. MA0: 100% Ca; MA90: 10% Ca; MA99: 1% Ca; MA100: 100% Mg; mole fractions of the metal components were calculated as the mole ratio of the corresponding metal component (Mg or Ca) to the total metal components in the catalyst. (b) Proposed process for the oxidative coupling of methane by surface oxygen species. O<sub>ads</sub>: adsorbed oxygen and O<sub>lat</sub>: lattice oxygen.<sup>71</sup> Reprinted with permission from ref. 71. Copyright © 2021, Elsevier.

compared with a type of mixed Ga–B oxide that exhibited Brønsted acidity.<sup>72</sup> They discovered that Ga<sub>4</sub>B<sub>2</sub>O<sub>9</sub> with the mullite-type structure exhibited intrinsic Lewis basicity, which was proved by CO<sub>2</sub>-TPD and DFT calculations despite its local superstructure, and then it was further proposed that the μ<sub>3</sub>-O atoms (linked to 3 metal atoms) linked with 5-coordinated Ga<sup>3+</sup> exclusively are likely the active sites in basic catalytic reactions and the origin of the strong basicity due to the structure-induction. Nevertheless, Ga<sub>4</sub>B<sub>2</sub>O<sub>9</sub> with fewer basic sites of 23.1 μmol g<sup>−1</sup> exhibited superior catalytic efficiency to Ga-PKU-1 (mixed Ga–B oxide) with larger acidic sites of 68.9 μmol g<sup>−1</sup>, suggesting that the process *via* base catalysis is more efficient.<sup>72</sup> Two years later, their group investigated the structure–performance correlation of Ga<sub>4</sub>B<sub>2</sub>O<sub>9</sub> (prepared by high-temperature solid-state reaction) in the Knoevenagel condensation reaction (several aldehydes with malononitrile to form α,β-unsaturated compounds through nucleophilic addition) more in-depth, which showed a high yield of 90% and high stability.<sup>73</sup> Their conclusions in earlier research were evidenced in this work by the structural comparison together with the catalytic activity among Ga<sub>4</sub>B<sub>2</sub>O<sub>9</sub>, GaBO<sub>3</sub> and β-Ga<sub>2</sub>O<sub>3</sub>. Because the O<sup>2−</sup> in the distorted GaO<sub>5</sub> (above-mentioned μ<sub>3</sub>-O) showed a relatively lower Bader charge, an electrophilic molecule, *i.e.*, malononitrile, was adsorbed and activated, and then the corresponding carbanion emerged by seizing one proton from the reactants. Then the activated reactant underwent nucleophilic attack by the carbanion at the Ga site adjacent to μ<sub>3</sub>-O.<sup>73</sup> Accordingly, it is evident that various strengths of basic sites

can provide different catalytic performances when designing catalysts, and well-developed oxygen vacancies and an abundance of specific basic sites are critical factors in designing efficient and high-performance catalysts.

In contrast with the previous description, in many cases, the reaction mechanism of mixed oxides may be not only base-catalyzed but synergistic. However, this should not be confused with the coexistence of acidic and basic phases in a single material. For example, in MgO–SiO<sub>2</sub>, during the conversion of bioethanol to butadiene, the acidic sites on silica or magnesium silicate are involved in the dehydration step, while the basic sites on magnesium oxide catalyse the dehydrogenation and condensation steps. These catalysts are bifunctional and the acidity and basicity described need to be characterized independently, with a possible optimal ratio between the acid and basic phases.<sup>74</sup> Moreover, the reaction mechanism for the ZrO<sub>2</sub> hydrogenation-catalyzed aromatic carboxylic acid generation of aldehydes is shown in Fig. 8, where the basic site extracts a proton from the carboxylic acid, the hydrogen adsorbs on the adjacent ion pair, and then isomerizes, the carboxylic acid radical and the negatively electrostatically charged hydrogen ion generates an aldehyde molecule, and then desorbs, and the adsorbed O<sup>2−</sup> forms water with the two hydrogen protons adsorbed on the lattice oxygen, and then desorbs, showing a synergistic effect. Another example is the mixed oxide of MgO and TiO<sub>2</sub>, where the number of basic sites decreases and the number of acidic sites gradually increases with an increase in the specific gravity of TiO<sub>2</sub>. When this catalyst was used for the alkylation reaction, it was found that the best catalytic effect was achieved when the specific gravity of the two mixtures was 1 : 1. The mixture has both acidic and basic sites at this specific gravity, and thus it is considered that the use of MgO–TiO<sub>2</sub> in this reaction causes it to proceed *via* an acid–base synergistic mechanism.<sup>75,77</sup>

Wang *et al.* synthesized a series of Ni/Ca<sub>x</sub>Mg<sub>y</sub>O catalysts composed of Ni nanoparticles and CaO–MgO mixed oxides to upgrade *n*-butanol into branched 2-ethyl-1-hexanol. By varying the content of surface Ni<sup>0</sup>, the *n*-butanol conversion increased obviously from 31.1% to 62.0% with an increase in Ni<sup>0</sup> concentration, evidencing the critical role of metal sites during the Guerbet reaction. By selectively poisoning the base sites using various amounts of benzoic acid, the conversion of *n*-butanol and the yield of 2-ethyl-1-hexanol decreased, while

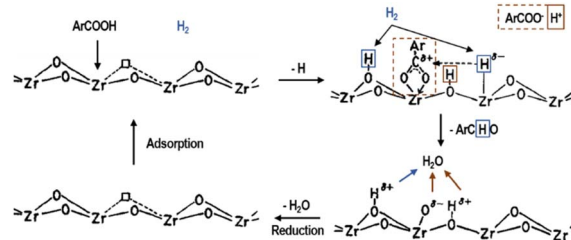


Fig. 8 Reaction mechanism of aromatic carboxylic acids to aldehydes catalyzed on ZrO<sub>2</sub> in the presence of hydrogen.<sup>75</sup> Adapted with permission from ref. 75. Copyright © 1992, Elsevier.





the yield of butyraldehyde increased slowly first, and then drastically. This indicates that the base sites serve as the active site in the Guerbet reaction, and also govern the catalytic activity in the aldolization. Research on the reaction duration and reaction temperature indicated that the highest conversion and yield of *n*-butanol dehydrogenation could reach 80.2% and 63.4%, respectively. Most notably, they confirmed that the dehydrogenation of *n*-butanol was the rate-determining step in the whole reaction process through the study of the structure–activity relationship and the reaction mechanism proposed, as shown in Fig. 9, in which the synergistic catalytic role of the Ni<sup>0</sup> site (metal site) and the base site was obviously reflected.<sup>76</sup>

**3.3.3 Performance in hydrocarbon cracking.** Metal oxides not only act as heat carriers in reactions but can also play a catalytic role. Preliminary studies on the use of vanadate and oxide-based catalysts for the thermal cracking reaction of hydrocarbon molecules have shown that the use of solid bases can promote the initial reaction, and thus lead to a limited increase in the conversion of the reaction; meanwhile, there will be less coking and carbon deposition on solid base catalysts than on solid acid catalysts during the cracking of hydrocarbon molecules due to the presence of substances such as loaded oxides. This has been partially studied by researchers in the field of petroleum refining using model compounds such as alkaline earth compounds that are highly active for gasification coke.<sup>79–82</sup> To date, their catalytic performance in the production of low-carbon alkanes and naphtha, and reactions with heavy oil as the feedstock.

**3.3.3.1 Low-carbon alkane catalytic cracking.** Kolts *et al.* examined the catalytic performance of MgO solid bases loaded with Mn and Fe, respectively, using *n*-butane as the feedstock. It was found that the use of solid bases significantly increased the conversion of the reaction and improved the selectivity for ethylene and ethane, while decreasing the selectivity for propylene by about 20%. Based on the results of the EPR and XRD characterization, it was found that the number of ethyl radicals increased and the number of MnO crystals decreased in the system after using the solid base catalyst, and thus the mechanism of *n*-butane cracking reaction and catalyst reduction process was proposed, as shown in Fig. 10. It was hypothesized that the use of a solid base led to an increase in the

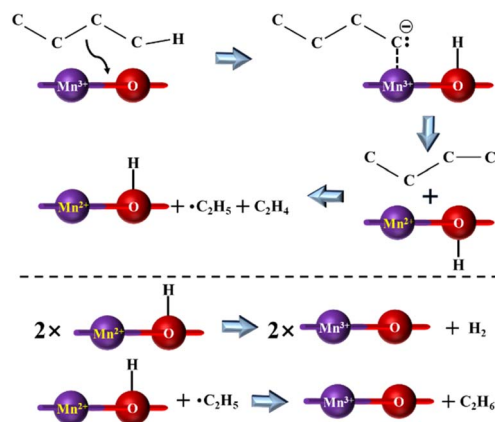


Fig. 10 Proposed mechanism for the selective cracking of *n*-butane over the Mn–MgO catalyst.<sup>78</sup> Adapted with permission from ref. 78. Copyright © 1986, AAAS.

content of major carbanions and charge transfer, thus facilitating the cracking reaction. The different product distributions that occur in cracking the two types of butanes also indicate differences in the stability of the carbanions produced by different feedstocks.<sup>78</sup> Co/Al<sub>2</sub>O<sub>3</sub> prepared by impregnation also provided high *n*-butane conversion in the oxidative cracking of *n*-butane, while N-Co/γ-Al<sub>2</sub>O<sub>3</sub> could provide up to 82% *n*-butane conversion at 600 °C, and this conversion value was higher than that from thermal cracking at 800 °C. XRD characterization revealed that the introduction of N promoted the formation of oxynitride and enhanced the mobility of oxygen. Different types of oxygen were responsible for different hydrocarbon molecule conversion pathways, and the high activity of lattice oxygen in CoO is the main reason for promoting the base-catalyzed dehydrogenation process to produce olefins.<sup>83</sup> In a study applying solid bases to the oxidative cracking of hexane, Li/MgO prepared using different methods exhibited different reaction properties, where the catalyst prepared by the sol–gel method provided about 28 mol% hexane conversion under the reaction condition at 575 °C and significantly improved the selectivity of low carbon olefins. Boyadjian *et al.* suggested that Li/MgO enhanced H capture by providing reactive oxygen sites, further increasing the production of olefins and free radicals, while Li/MgO prepared *via* the sol–gel method can further promote the oxidative cracking of hexane by providing a larger surface area and more active sites.<sup>85</sup>

The recent study by Wang *et al.* suggested that the combination of metal sites and mobile oxygen species on Y<sub>2</sub>O<sub>3</sub>-modified Au–La<sub>2</sub>O<sub>3</sub> catalysts provided superior activity for catalytic *n*-propane oxidative cracking and the synthesized catalysts showed stable activity over 24 h without significant deactivation.<sup>84</sup> According to the H<sub>2</sub>-TPR results, as shown in Fig. 11(a), the combined sites arising from the metal-support interactions and 5Y-0.2Au–La<sub>2</sub>O<sub>3</sub> (impregnation of calculated amount of 0.2Au–La<sub>2</sub>O<sub>3</sub> in yttrium nitrate equivalent to 5 wt% yttrium oxide, Au (0.2 wt%) supported on La<sub>2</sub>O<sub>3</sub> marked as 0.2Au–La<sub>2</sub>O<sub>3</sub>, where the same applies below) exhibited a high-intensity reduction peak. It is known that Y<sub>2</sub>O<sub>3</sub> and La<sub>2</sub>O<sub>3</sub> are

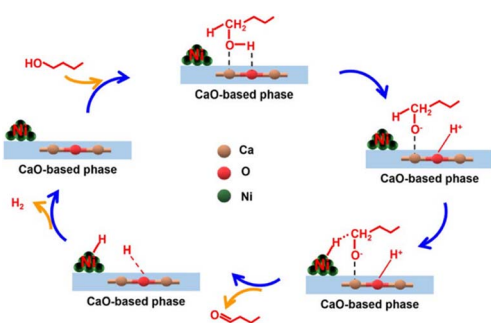


Fig. 9 Synergistic catalysis reaction mechanism *via* the metal and base sites for the dehydrogenation of *n*-butanol.<sup>76</sup> Reprinted with permission from ref. 76. Copyright © 2020, the American Chemical Society.



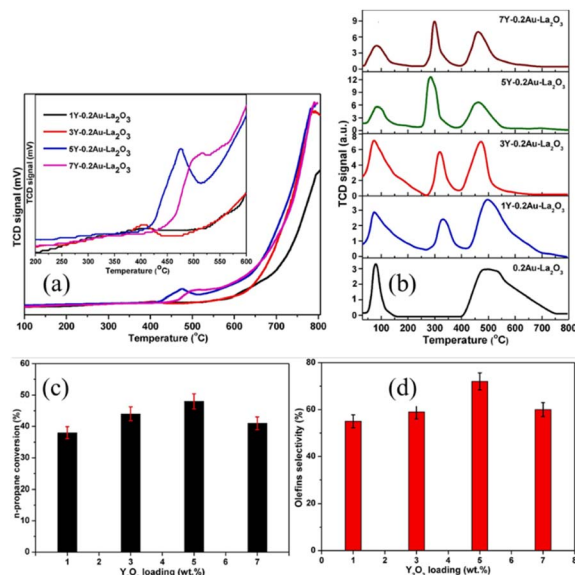


Fig. 11 (a) H<sub>2</sub>-TPR and (b) O<sub>2</sub>-TPD patterns of synthesized samples. Reaction activity tests of the catalysts. The influence of Y<sub>2</sub>O<sub>3</sub> loading on (c) conversion of *n*-propane and (d) selectivity to olefins. Reaction conditions: 500 °C; GHSV: 48 000 h<sup>-1</sup>.<sup>84</sup> Reprinted with permission from ref. 84. Copyright © 2020, Elsevier.

basic in nature and can have intimate contact with gold metal nanoparticles to generate active sites.<sup>86</sup> The O<sub>2</sub>-TPD results, as shown in Fig. 11(b), demonstrated three peaks, where the two main peaks are attributed to the desorption of different oxygen species (*e.g.*, surface O<sub>2</sub><sup>-</sup> and/or O<sub>2</sub><sup>2-</sup> species), surface and bulk lattice oxygen species of metal oxides from low-temperature to high-temperature, respectively. Among them, 5Y-0.2Au-La<sub>2</sub>O<sub>3</sub> showed the highest desorption peaks, indicating the presence of more oxygen supplying centers. Meanwhile, the reaction activity improved after loading 1–5 wt% of Y<sub>2</sub>O<sub>3</sub> on the carriers, suggesting that Y<sub>2</sub>O<sub>3</sub> is a major factor in this improvement, as shown in Fig. 11(c and d). It was reported that the olefin molecules desorb faster over the basic oxides, which could halt olefin dissociation and improve the olefin selectivity.<sup>87</sup> Consequently, 5Y-0.2Au-La<sub>2</sub>O<sub>3</sub> delivered superior activity with the *n*-propane conversion of 78% and olefin selectivity of 72% due to its ease of reduction and more mobile oxygen species and metal sites.<sup>84</sup>

However, the above-mentioned studies on the cracking of low-carbon alkanes using solid bases revealed that the production of CO<sub>x</sub> can poison the catalysts and reduce the selectivity of low-carbon olefins, and the combustion of low-carbon olefins may occur during the oxidative cracking reaction, thus making it difficult to control the reaction process.<sup>84,88</sup>

**3.3.3.2 Naphtha catalytic cracking.** Jeong *et al.* used KVO<sub>3</sub>/Al<sub>2</sub>O<sub>3</sub> prepared *via* the impregnation method, and then used it in the catalytic pyrolysis reaction of naphtha at 800 °C.<sup>89</sup> They found that the use of this solid base significantly improved the yields of ethylene and propylene, while the yield of low carbon olefins was found to be almost the same when Al<sub>2</sub>O<sub>3</sub> alone was used in the same reaction as that of the KVO<sub>3</sub>/Al<sub>2</sub>O<sub>3</sub> catalyst.

This indicates that the cracking performance is mainly dependent on the Al<sub>2</sub>O<sub>3</sub> component, while KVO<sub>3</sub> is responsible for reducing the carbon deposition, as shown in Table 3 for the CO<sub>x</sub> products and carbon deposition of the series catalysts. Also, they suggested that the introduction of KVO<sub>3</sub> increased the coking gasification rate to suppress carbon deposition.<sup>89</sup> Since then, Jeong *et al.* introduced B<sub>2</sub>O<sub>3</sub> in the above-mentioned solid base to investigate the anti-carbon deposition ability of these catalysts. The introduction of B<sub>2</sub>O<sub>3</sub> was found to enhance the stability of the alkali metal K in the reaction according to the ICP-AES characterization, and the main reason for the stabilization of K by TPR was the strong interaction of B<sub>2</sub>O<sub>3</sub> with KVO<sub>3</sub>.<sup>81</sup>

Previously, Pierre L. *et al.* studied the catalytic thermal cracking of naphtha with metal oxide mixtures as catalysts for the purpose of producing more low carbon olefins, with the main components of MgO, SiO<sub>2</sub>, ZrO<sub>2</sub>, and small amounts of Nd<sub>2</sub>O<sub>3</sub>, Al<sub>2</sub>O<sub>3</sub>, and CaO. The results showed that the catalysts were stable at the bed temperature of 650–900 °C and the corresponding pressure, with high ethylene yield and no carbon deposition, and the catalysts did not require regeneration.<sup>90</sup> Thereafter, Lemonidou *et al.* showed that 12CaO–7Al<sub>2</sub>O<sub>3</sub> had the highest yield of low carbon olefins and the lowest yield of CO<sub>x</sub> in a study on *n*-hexane cracking using various mixed metal oxides, while the conversion of *n*-hexane started to decrease after reduction of the catalyst, which proved that the active oxygen in the catalyst acted as a base active center. This is also the reason why calcium aluminate catalysts have been more applied and studied in the research on solid base catalysts used in the field of catalytic cracking.<sup>91</sup> When 12CaO–7Al<sub>2</sub>O<sub>3</sub> was used for naphtha catalytic cracking, the reaction temperature could be reduced by 50 °C compared to the steam cracking process, and it also reduced the catalyst carbon deposition by promoting the gasification of coke, but the use of 12CaO–7Al<sub>2</sub>O<sub>3</sub> did not affect the product distribution.<sup>92</sup> Mukhopadhyay *et al.* introduced K<sub>2</sub>CO<sub>3</sub> in 12CaO–7Al<sub>2</sub>O<sub>3</sub> and found that the carbon deposition decreased with the loading of K<sub>2</sub>CO<sub>3</sub>, but the yield of low carbon olefins also decreased slightly, and they suggested that the combination of K and reactive oxygen species occupied the active site of the cracking.<sup>93</sup> Kumar *et al.* studied the effect of calcium aluminate catalysts with K introduced by different preparation methods on the cracking performance of *n*-heptane and the amount of loaded metal, and found that calcium aluminate catalysts significantly improved the ethylene yield of *n*-heptane pyrolysis. Also, they showed that the introduction of K promoted the gasification of carbon deposits and the K-

Table 3 CO<sub>x</sub> and coke yield of catalysts in catalytic pyrolysis of naphtha at 800 °C.<sup>89</sup> Used with permission from ref. 89. Copyright © 2001, the American Chemical Society

Catalysts	Yield of CO <sub>x</sub> (wt%)	Yield of coke (wt%)
α-Al <sub>2</sub> O <sub>3</sub>	1.96	0.51
KVO <sub>3</sub> /α-Al <sub>2</sub> O <sub>3</sub>	2.87	0.17
KVO <sub>3</sub> –B <sub>2</sub> O <sub>3</sub> /α-Al <sub>2</sub> O <sub>3</sub>	2.92	0.14



loaded calcium aluminate catalysts prepared by impregnation method had high cracking activity, but the amount of K loading was easily lost with an increase in the reaction time.<sup>94</sup> T. Tomita *et al.* studied the naphtha cracking reaction of alkaline earth metal oxides or their mixtures co-sintered with alumina to prepare solid bases and concluded that alkaline earth metal oxides can inhibit the hydrocarbon dehydrogenation reaction and inhibit the thermal polymerization reaction. This is important for the inhibition of carbon deposition; meanwhile, CaO and Al<sub>2</sub>O<sub>3</sub> co-crystals can form a spinel-like structure, which remains stable at 800 °C.<sup>95</sup>

The aforementioned studies on the application of mixed metal oxide catalysts in catalytic cracking almost came to a halt around the twentieth century, but due to their good resistance to carbon deposition, they are beginning to become important in the present environment of heavy and inferior crude oil.

**3.3.3.3 Heavy oil catalytic cracking.** Tian *et al.* used FCC catalysts with calcium aluminate catalysts for the catalytic cracking of vacuum residue oil and found that although the FCC catalysts resulted in higher conversion at the same temperature, their high dry gas yield and low liquid yield compared to calcium aluminate catalysts indicated that they may be more likely to lead to over-cracking of the oil, while having about twice the carbon deposition yield than calcium aluminate catalysts.<sup>96</sup> Tang *et al.* compared the distribution of low-carbon olefin products after the catalytic cracking of vacuum residue oil with FCC catalysts and calcium aluminate catalysts, and then found that calcium aluminate had higher low-carbon olefin yields at 650 °C.<sup>97</sup> They further investigated the catalytic ability of magnesium aluminate and calcium aluminate for cracking vacuum residue oil and found that both types of catalysts were favorable for improving the yield of low carbon olefins, while calcium aluminate was superior. They suggested that the catalysts promoted the generation of free radicals by hydrogen abstraction of the reactants, and thus improved the yield of low carbon olefins. Thus, to improve the base density of calcium aluminate, they created a porous structure in calcium aluminate by adding graphite and several types of organic substances, which improved the conversion of heavy oil to light oil, and they proposed that the porous structure formed on calcium aluminate facilitated the distribution of reactive oxygen species and increased the contact probability of reactants with the active center.<sup>98,99</sup> Recently, Niwamanya *et al.* studied the catalytic cracking of heavy oil using the above-mentioned catalysts and found that the strong basicity of calcium aluminate promotes hydrocarbon dehydrogenation and its yield of low carbon olefins is higher compared to quartz sand, but its conversion, low-carbon olefin yield, and aromatic yield are lower compared to the acidic catalyst ZSM-5. Accordingly, they proposed the combination of calcium aluminate and ZSM-5 in an optimized ratio and concluded that only a suitable ratio can provide a suitable acid center concentration. Compared with the general FCC catalysts with ZSM-5 and Y-type zeolites as the main active components, these combinations can better balance the shape selectivity, cracking and hydrogen transfer activities of the catalysts, and thus obtain relatively high low-carbon olefin and aromatic yields.<sup>15</sup>

In summary, among the loaded oxides, researchers are currently focusing their efforts on calcium aluminate catalysts. Their early application was aimed at reducing carbon deposition in the steam cracking process, and their characteristics may make them suitable for the treatment of heavy and inferior heavy oils. Some studies on loaded solid base catalysts have confirmed that the use of these catalysts can indeed promote the cracking reaction of prolific olefins to some extent, and it is recognized that the introduction of alkali metal compounds in alkali metal oxides has a significant effect on the reduction of carbon deposition in catalysts. However, because of the aforementioned drawbacks, only a few loaded solid base catalysts that can catalyze the cracking reaction have been developed thus far, and their research has been stalled for a while. Besides, using mixed metal oxides in combination with zeolites may be another way forward for the efficient green treatment of heavy oil.

## 4 Zeolite-based solid bases

Zeolites have attracted significant attention because of their regular pore structure and high specific surface area, and they have also been studied by scientists from various countries because of their good shape-selective catalytic ability, and the selection of zeolites as carriers for basic shape-selective catalysis is an important step in the preparation of solid base catalysts and the realization of new green catalytic processes.<sup>17</sup>

### 4.1 Ion-exchange of alkali metals

**4.1.1 Intrinsic properties.** In the preparation of solid base materials using zeolites as carriers, only weak basic zeolites can be obtained by alkali metal ion exchange, while loading the zeolite with more alkali metal ions than its ion exchange number may produce a more basic zeolite. Unlike the aforementioned mixed oxides, whose basicity between that of their components, the basicity of solid base catalysts prepared by direct doping or loading of alkali metals on zeolites can exceed the basicity of the loaded alkali metal oxides, and the base strength of the prepared solid base catalysts is enhanced to some extent compared with that of each component.<sup>101,102</sup> However, it is still difficult to obtain strong basic sites on zeolites by modification because of various unknown factors, and thus far there are few reports on the industrial applications of solid base catalysts prepared with zeolites as carriers. Thus, the preparation of solid base zeolites for catalysis has become a weak and difficult point in the study of zeolite shape-selective catalysis.

In the majority of situations, the catalytic activity of the basic sites of zeolites after alkali metal ion exchange is positively correlated with the atomic number of alkali metal ions and negatively correlated with the silica-alumina ratio of the zeolite framework, and this can be explained by the change in the negative charge of the lattice oxygen. The negative charge number of the lattice oxygen can be calculated by the Sanderson electronegativity equilibrium theory, which is an effective method to determine the basicity strength of alkali metal ion-





exchanged zeolites.<sup>103–105</sup> The framework oxygen binding energy (BE) in the XPS characterization method corresponds to the electronic charge of the lattice oxygen, as shown in Fig. 12(a), demonstrating the relationship between the lattice oxygen binding energy of X- and Y-type zeolite and the electronegativity of the metal cation. The electronegativity of the exchange cation and the silica-alumina ratio of the framework are positively correlated with the binding energy BE of the lattice oxygen, respectively. The weaker the binding energy of the lattice oxygen, the stronger its electron-donating capacity and the basic strength. Meanwhile, Okamoto *et al.* argued that the basic sites of zeolites originate from the lattice oxygen after ion-exchange and proposed a bonding model of exchange ions, as shown in Fig. 12(b), where two possible binding states exist after ion exchange, covalent bonding between cation-oxygen and ionic bonding formed by the negative charge of the leaving group on cation-aluminium, and basicity is related to the ionic bonding mode, while the bonding mode in general is a mixture of these two types of bonding modes.<sup>4,100,106</sup>

The zeolite exchanged by alkali metal ions has a negative oxygen charge number, and the order of its basicity is Cs, Rb, K, Na, and Li according to the negative charge number from the largest to the smallest, then the order of its basicity is Cs, Rb, K, Na, and Li from the largest to the smallest. The negative oxygen charge number of the zeolite exchanged by the same alkali metal ions increases with a decrease in the silica-alumina ratio of the framework, *i.e.*, the smaller the silica-alumina ratio, the stronger the basicity of the modified zeolite. The basicity of zeolites is not only related to their intrinsic structure and the type of metal ions loaded but also their chemical environment, the distribution of aluminium on the framework, and the position of the metal cations.<sup>107</sup>

As can be seen from the above-mentioned investigation, alkali metal ion-exchanged zeolites have a lower base strength than that exchanged with alkaline earth metal oxide, and also lower than that of zeolites exchanged with an alkali metal compound, exceeding the ion exchange capacities of the zeolite. Although alkali metal ion-exchanged zeolites have a lower strength of basic sites, their base strength can be adjusted by different cation exchanges, and thus the zeolite after ion exchange can be better suited for multiple types of reactions.

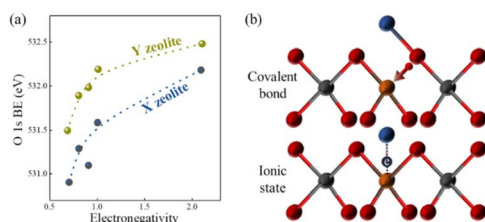


Fig. 12 (a) Relationship between the O 1s binding energy of lattice oxygen and the electronegativity of cation-exchanged X and Y zeolites. (b) Proposed bonding models on zeolites after cation-exchange. Red sphere: O, grey sphere: Si, brown sphere: Al, and blue sphere: metal cation.<sup>100</sup> Adapted with permission from ref. 100. Copyright © 1988, Elsevier.

**4.1.2 Performance in fine chemical catalysis.** Earlier studies found that Faujasite zeolites exchanged with alkali metal ions such as Cs<sup>+</sup> and Rb<sup>+</sup> had good selectivity and conversion for the reaction of toluene with methanol/formaldehyde side chain alkylation to produce styrene and ethylbenzene, while the X-type zeolite activity was higher than the Y-type zeolite in the ion-exchanged octahedral zeolites.<sup>108</sup> Usually, benzene alkylation occurs on acidic catalysts and side-chain alkylation occurs on basic catalysts. Therefore, the above-mentioned reactions indicate that after the exchange of alkali metal ions, the zeolite has basic sites and acts as a base catalyst for this reaction. These observations have prompted researchers to investigate the alkali modification and catalytic properties of alkali metal ion-exchanged zeolites more in-depth.

The catalytic properties of alkali metal ion-exchanged zeolites depend on their weak base sites and regular pore channels. It was found that although the regular pore structure can produce shape-selectivity, it can also have an effect on the diffusion of reactants and products, especially in liquid-phase reactions involving solid bases, and thus researchers aimed to use exchange ions with different radii or electronegativities to modulate their basicity.<sup>109</sup> In the application of X-type zeolites loaded with K<sup>+</sup>, Cs<sup>+</sup>, and Na<sup>+</sup>, respectively, in the reaction of dehydration and dehydrogenation of 2-propanol, the active sites of base catalysis were attributed to the loading of the three cations. Specifically, K<sup>+</sup> and Cs<sup>+</sup> were more likely to produce basic sites than Na<sup>+</sup>, and thus dehydrogenation mainly occurred on KX and CsX, while the dehydration reaction occurred on NaX.<sup>110,111</sup> In the MPV (Meerwein-Ponndorf-Verley) reduction of aldehydes with 2-propanol to produce the corresponding 1-alcohol over NaX, the framework oxygen adjacent to Na<sup>+</sup> abstracts a proton from 2-propanol, and the oxygen acts as the base center.<sup>112</sup> The replacement of Si in NaX by Ge can produce relatively stronger basic sites, enhancing its catalytic activity in the Knoevenagel condensation reaction.<sup>113,114</sup> However, Corma *et al.* suggested that the origin of the enhanced activities is the smaller T–O–T (intrinsic chemical bond formation with oxygen inside zeolite) bond angle, longer T–O bond, and larger cell size after the replacement of Si by Ge. The activity of the NaGe Faujasite is higher than that of pyridine and lower than that of piperidine, indicating that most of the basic sites on the NaGeX zeolite have a  $pK_b$  of about 11.2 and basic sites with strength in the order of  $pK_b$  of 13.3 should exist to abstract protons from ethyl malonate.<sup>115</sup> In summary, although the ion-exchange can alter the negative charge of the zeolite framework, it is still difficult to prepare strong base materials *via* this method.

## 4.2 Loading alkali metals

**4.2.1 Intrinsic properties.** The main methods for loading alkali metals on zeolites are the direct loading of zeolites in alkali metal vapor or impregnation of zeolites with alcohol solutions of alkali metal azides, followed by calcination to decompose the azide loading. Different preparation methods result in different states of the loading alkali metals, with higher heating rates (25 °C min<sup>−1</sup>) producing ionic clusters and lower heating rates (1 °C min<sup>−1</sup>) producing neutral clusters.<sup>116</sup>



For example, when Y-type zeolites are impregnated with methanolic solutions of sodium azide and calcined at different temperatures, alkali metals can exist in three states, *i.e.*, large  $\text{Na}_x^0$  particles outside the crystal, neutral  $\text{Na}_y^0$  atomic clusters inside the crystal and  $\text{Na}_4^{3+}$  ionic clusters inside the square sodium stone cage. Although clusters are generated during catalyst preparation, it has been proposed that the basic frame oxygen negative ions near the neutral Na atom clusters are basic sites, and thus there is a controversy about whether the clusters are the active sites for base catalysis.<sup>117</sup> It is worth noting that loading alkali metals is more effective than loading their oxides in the preparation of strongly basic sites, where the loading of alkali metals can increase the number of base centers, but it does not necessarily have a good effect on the improvement of the intensity of the base centers. For example, Na/NaX is more basic than  $\text{NaO}_x/\text{NaX}$ , and the improvement in Na loading on NaX increases the amount of  $\text{CO}_2$  adsorption sites, but with an increase in the Na loading, the maximum values of base intensity did not show a significant improvement.<sup>118,119</sup>

**4.2.2 Performance in fine chemical catalysis.** A characteristic of base catalysis that differs from acid catalysis is that although the basicity of the solid base does not change significantly, its activity and selectivity can change significantly when applied to certain reactions.

Good catalytic activity was observed in side-chain alkenylation reactions at lower reaction temperatures on zeolites loaded with K, Na, and Cs with azide compounds as intermediates, while the reaction was difficult to occur on CsX zeolites loaded with  $\text{CsO}_x$ .<sup>120</sup> When the Michael addition reaction of ethyl acrylate with acetone was catalyzed using modified zeolites at 90 °C, Na/NaX showed the best catalytic activity, followed by  $\text{CsO}_x/\gamma\text{-Al}_2\text{O}_3$ , Na/NaOH/ $\gamma\text{-Al}_2\text{O}_3$ , and  $\text{CsO}_x/\text{CsX}$ , while NaX and CsX had no catalytic activity. The Hammett indicator of the modified zeolites was  $\text{CsO}_x/\gamma\text{-Al}_2\text{O}_3$  (>37), Na/NaOH/ $\gamma\text{-Al}_2\text{O}_3$  (35–37),  $\text{CsO}_x/\text{CsX}$  (17.2–18.4), and NaX (<9.3), and the base strength sequencing is consistent with the catalytic activity sequencing.<sup>121</sup> The decomposition performance of a series of catalysts prepared with  $\text{NaN}_3$  as precursor loaded with Na on different zeolites and  $\text{Al}_2\text{O}_3$  for the base-catalyzed reaction of MBOH decomposition to acetone followed the order of NaX > NaY > NaL > Naβ >  $\text{Al}_2\text{O}_3$ , and the difference in reactivity was attributed to the different types of zeolite carriers.<sup>3</sup>

According to the aforementioned studies, it can be concluded that the catalytic process of base catalysis is more sensitive to the properties of the basic site of the solid base rather than the strength and density of the base. It was demonstrated that some reactions could not proceed on zeolites with alkali metal ion exchange or loaded with alkali metal oxides, but good reactivity could be achieved *via* alkali metal loaded zeolites.

### 4.3 Loading alkali metal oxides

**4.3.1 Intrinsic properties.** As described in Section 4.1, the basicity of zeolites can be enhanced by loading with several alkali metal ions exceeding their ion exchange capacity, and alkali metals can form alkali metal clusters on zeolites and

these modified zeolites are strongly basic solid bases. This is mainly due to the formation of strongly basic sites in the pore channels of alkali metal oxides or frame oxygen adjacent to alkali metal atom clusters in zeolites after alkali metal loading.<sup>123</sup>

The basic sites of an X-type zeolite after ion exchange exceeding the exchange capacity of cesium acetate are  $\text{Cs}^+$  introduced by ion exchange or within the supercage of the zeolite and  $\text{Cs}_2\text{O}$  loaded within its pore channel.<sup>124</sup> Unlike  $\text{Cs}^+$  ion exchange, excess  $\text{Na}^+$  will be located in the hexagonal column away from the outer surface rather than inside the supercage. Yagi *et al.* conducted an in-depth study on the relationship between Cs content and basic sites on type X zeolites by  $^{133}\text{Cs}$  MAS NMR characterization and the results showed that if the number of Cs atoms in the supercage is greater than the exchangeable capacity of the X-type zeolite but not greater than 2.9, the  $\text{Cs}^+$  that is added greater than the exchangeable capacity exists in the pore cavity of the supercage on the zeolite. Alternatively, if it is more than 2.9, the  $\text{Cs}^+$  exceeding the exchangeable capacity part is distributed on the outer surface of the zeolite.<sup>125</sup> The solid base obtained by ion exchange of  $\text{Cs}^+$  with the Y-type zeolite, and then impregnated with CsOH has  $\text{Cs}^+$  on the exchangeable ion sites in addition to the oxide species of Cs. Hunger *et al.* suggested that the Cs oxides within the zeolite did not form large clusters but highly dispersed oxide species on the surface of the zeolite.<sup>126</sup> Further, the  $^{18}\text{O}_2$ -TPD studies showed that the surface layer of  $\text{Cs}_2\text{O}$  partially forms peroxide or superoxide such as  $\text{Cs}_2\text{O}_2$ ,  $\text{Cs}_2\text{O}_3$ , and  $\text{Cs}_2\text{O}_4$ , which in turn may produce strongly basic sites. The oxides formed by these solid bases after the adsorption of oxygen all exhibit structural features of  $\text{Cs}^+$  bonding to  $\text{O}_2^-/\text{O}_2^{2-}$  with negatively charged oxygen atoms in the adsorbed oxygen. The bonding model diagram of  $\text{Cs}_2\text{O}_2$  and  $\text{Cs}_2\text{O}_4$  generated after the adsorption of oxygen is shown in Fig. 13. The oxygen atom can be decoupled without breaking the chemical bond between the two oxygen atoms in the peroxide or superoxide when the peroxide and superoxide are reduced to  $\text{Cs}_2\text{O}$  through the rearrangement of Cs and O.<sup>122,124</sup> In summary, different pretreatment conditions can lead to different oxygen environments, and different chemistry states of cesium oxide may exist in solid bases such as superoxide  $\text{CsO}_2$ , peroxide  $\text{Cs}_2\text{O}_2$ , oxide  $\text{Cs}_2\text{O}$ , low oxygenated  $\text{Cs}_7\text{O}$ , and metallic Cs.

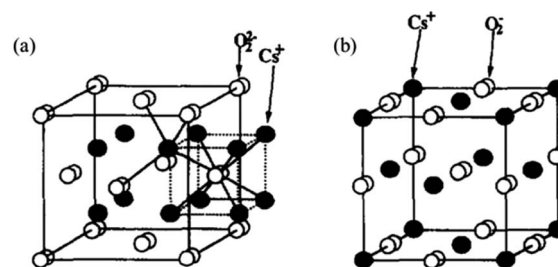


Fig. 13 Bonding structures of various cesium oxides. (a)  $\text{Cs}_2\text{O}_2$  and (b)  $\text{Cs}_2\text{O}_4$ .<sup>122</sup> Reprinted with permission from ref. 122. Copyright © 1997, Elsevier.



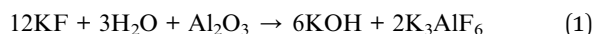
**4.3.2 Performance in fine chemical catalysis.** Alkali metal oxide-loaded zeolites have stronger basicity than ion-exchange zeolites, and there is a significant difference in their application in 1-butene isomerization, while the solid bases prepared by loading  $\text{CsO}_x$  has the strongest base strength among the alkali metal ion-loaded zeolite, and the catalytic activity follows the order of  $\text{CsO}_x/\text{CsX} > \text{CsO}_x/\text{KX} > \text{KO}_x/\text{KX}$ .<sup>127,128</sup> After vacuum pretreatment at 500 °C, the basicity of  $\text{KNO}_3/\text{KL}$  is enhanced and it can be used to catalyze the isomerization of *cis*-2-butene.<sup>129</sup> During the decomposition of 2-propanol catalyzed by  $\text{NaO}_x/\text{NaX}$ , it was found that there was a significant positive correlation between the formation rate of acetone and the loading of  $\text{NaO}_x$ . At 240 °C, the acetone selectivity of the  $\text{NaX}$  zeolite and  $\text{NaX}$  zeolite supported by  $\text{NaO}_x$  was 24% and more than 90%, respectively. There was a significant negative correlation between the loading of  $\text{NaO}_x$  and the formation rate of propylene, which was because the loading of  $\text{NaO}_x$  neutralized its surface acidic center. Simultaneously, with the loading of  $\text{NaO}_x$ , its dehydrogenation ability gradually increased, indicating that the basicity increases with an increase in the  $\text{NaO}_x$  loading and produces some strong basic sites.<sup>119</sup> The catalytic performance of propanol dehydrogenation was significantly improved after loading  $\text{CsO}_x$  on  $\text{CsY}$ . Due to the large specific surface area of the zeolite, the catalytic activity per unit weight of  $\text{Cs}/\text{NaY}$  loaded with  $\text{Cs}_2\text{O}$  was about 6 times that of the metal oxide  $\text{MgO}$ .<sup>130</sup> Due to the strong basicity of  $\text{CsO}_x/\text{MCM-41}$  and  $\text{CsO}_x/\text{MCM-48}$  pores by loading them with  $\text{CsO}_x$  particles, reactions such as Knoevenagel condensation and Michael addition have good activity under base catalysis, although the impregnation of the sample with cesium acetate after  $\text{Cs}^+$  exchange results in partial collapse of its structure, but will continue to improve its catalytic capacity.<sup>131,132</sup> In the cyclization of acetone to produce methyl-cyclopentanone and dimethylfuran, the acidity and basicity of the catalyst can be expressed in terms of the ratio of methyl-cyclopentanone to dimethylfuran, which is higher on basic catalysts. The modification of MCM-41 with  $\text{CsO}_x$  and  $\text{KO}_x$  gave only methyl-cyclopentanone between the main two types of products, demonstrating that MCM-41 can be converted to a solid base catalyst by modification.<sup>133,134</sup>

#### 4.4 Other loaded compounds

**4.4.1 Intrinsic properties.** The basic properties of traditional silica-alumina zeolites include silica-alumina ratio, chemical bond angle, and bond length, while the intrinsic basicity sites of zeolites are generally derived from their framework oxygen and  $\text{O}^{2-}$  ions adsorbed at defect sites. Generally, the basicity depends on the changes in the basic properties of the zeolites. After exchange with alkali metal, the basicity of zeolites is enhanced with a decrease in the silica-alumina ratio and increase in the radius of exchanged alkali metal ions, and the mainstream explanation for this change is that the introduction of the alkali metal changes the electron cloud density distribution in the zeolite framework and its cage, and the electronegativity is enhanced according to the acid-base electron theory to enhance the basicity of the zeolite.

Previously, studies on the base modification of zeolite materials have appeared, and among them, their modification with alkali metals, alkaline earth metals, and rare earth metals was confirmed to contribute to the improvement in the properties of zeolite materials and the promotion mechanisms of different metal oxides were classified as different catalytic mechanisms.<sup>12</sup> Although the actual preparation process showed that their basicity is affected by various factors differing from theory, researchers found that the reaction between the metal and frame silica occurs when oxides and hydroxides of alkali metals are directly loaded on zeolites, eroding their framework. This leads to the collapse or blockage of the framework or pores, and thus the selection of weakly basic precursors and neutral metal salts with weaker basicity will be an effective way to alleviate the collapse of the modified zeolites.<sup>3,135</sup>

KF,  $\text{KNO}_3$ , and  $\text{K}_2\text{CO}_3$  are weakly basic and neutral metal salts, and it has been shown that these three compounds loaded with  $\text{Al}_2\text{O}_3$  could produce strong solid base sites.<sup>136–138</sup> For example, KF-loaded  $\text{Al}_2\text{O}_3$  presented both stronger basicity and nucleophilicity than  $\text{KOH}/\text{Al}_2\text{O}_3$ , but its specific surface area remained at only about  $31 \text{ m}^2 \text{ g}^{-1}$  after treatment at 500 °C.<sup>139</sup> Zeolites are good carriers for KF loading because of their extremely high specific surface area and good shape-selecting ability.  $\text{NaY}$  has a high specific surface area of  $766 \text{ m}^2 \text{ g}^{-1}$ , and because silica-alumina zeolites have an elemental composition similar to  $\text{Al}_2\text{O}_3$  and  $\text{SiO}_2$ ,  $\text{NaY}$  can react similarly to the loading of  $\text{Al}_2\text{O}_3$  and  $\text{SiO}_2$  after loading KF, as shown in the following chemical eqn (1) and (2), which in turn produces a basic species similar to  $\text{KOH}$ .<sup>140</sup>



Although KF does not destroy the structure of the zeolite during synthesis, as evidenced by XRD characterization, the interaction of KF with the zeolite framework intensifies during high-temperature pretreatment, and KF can react with the silicon component of the zeolite framework to form low-intensity silica-potassium compounds, which leads to the collapse of the framework at high temperatures.<sup>138,141</sup> Also, because the zeolite contains a silicon component and the silicon component reacts preferentially with KF, resulting in a significantly lower base strength of  $\text{KF}/\text{NaY}$  ( $\text{H} < 9.3$ ) than that of  $\text{KF}/\text{Al}_2\text{O}_3$  ( $\text{H} > 17.2$ ), some experiments have shown that the base strength of KF loaded on a mixture of  $\text{Al}_2\text{O}_3$  and  $\text{SiO}_2$  is similar to that of  $\text{KF}/\text{SiO}_2$ . This indicates that the presence of a silicon component in the zeolite hinders the generation of strong basic sites, and simultaneously reduces the stability of the zeolite in hydrothermal treatment.<sup>140</sup>

Unlike KF modifications,  $\text{KNO}_3$  modification is not dependent on interaction with the zeolite carriers but can decompose itself to produce strongly basic sites, and thus  $\text{KNO}_3$  modification can greatly reduce the damage to the zeolite framework. The  $\gamma\text{-Al}_2\text{O}_3$  framework has octahedral vacancies that can hold cations, which are important to facilitate the decomposition of  $\text{KNO}_3$  to promote the production of strongly basic sites.<sup>142,143</sup>





Meanwhile,  $\text{KNO}_3/\gamma\text{-Al}_2\text{O}_3$  activation at a high temperature of 600 °C produced a much more basic site than the MgO basicity with  $\text{H}$  of about 27.0, but the specific surface area of  $\text{KNO}_3/\gamma\text{-Al}_2\text{O}_3$  after high-temperature activation was positively low, with only about  $80 \text{ m}^2 \text{ g}^{-1}$ , and thus zeolites with a high specific surface area are employed to improve the specific surface area of these solid bases.<sup>137,144</sup> However, the base amount of 21%  $\text{KNO}_3/\text{NaY}$  was only  $0.16 \text{ mmol g}^{-1}$  after pretreatment at 600 °C. Some studies showed that the variation between NaY and  $\gamma\text{-Al}_2\text{O}_3$  was due to the fact that NaY lacks important octahedral vacancies for embedding and adsorption of  $\text{K}^+$ , and the zeolite framework and surface may change and reform during pretreatment, and thus although  $\text{KNO}_3$  can be highly dispersed on NaY, it is difficult to thermally decompose and form strong base sites.<sup>142</sup>

Not only loading different K predecessors can change the physicochemical properties and catalytic characteristics of the catalyst, but it is also necessary to choose a suitable carrier. For example, Y- and KL-type zeolites have different structures despite similar silica-alumina ratios, and KL zeolites were modified by KF to obtain a basic center with  $\text{H}$  of only about 15 for KL zeolites.<sup>138</sup> After pretreatment of KL zeolite loaded with  $\text{KNO}_3$  or  $\text{K}_2\text{CO}_3$  at 600 °C at high temperature, it was found that the high-temperature decomposition of the compound on the surface of KL zeolite produced super basic sites with  $\text{H}$  of about 27.0. Some studies showed that the loaded  $\text{KNO}_3$  started to decompose at 500 °C during high-temperature pretreatment. The characteristic peaks of  $\text{NO}_2^-$  and KOH were not found by FTIR characterization, confirming that  $\text{K}_2\text{O}$ , not  $\text{KNO}_2$  and KOH, was produced when  $\text{KNO}_3$  was loaded on KL and pre-treated at high temperature. The  $\text{CO}_2$ -TPD characterization showed that the  $\text{CO}_2$  desorption temperature of 21%  $\text{KNO}_3/\text{KL}$  was higher than that of KL zeolite, while a new high-temperature desorption peak appeared at 500 °C, indicating that the basicity of the carrier was significantly changed and enhanced.<sup>145,146</sup>

According to the research on alkali-modified zeolites used in the traditional fine-chemical industry, intrinsic solid base materials generally have a smaller specific surface area, poorer mechanical strength, and weaker hydrothermal stability, while they do not have the regular pore structure and very high specific surface area of zeolite-based catalysts. Thus, in the petroleum industry, based on the research experience of solid bases in the traditional fine-chemical industry, the combination of basic active components and materials with regular pore structure has received more attention from researchers.

**4.4.2 Performance in fine chemical catalysis.** Although traditional strong solid bases such as metal oxides stated in the previous chapter tend to be deactivated by the deposition of coke, it is well known that supporting them on appropriate materials such as porous silica and zeolite can moderate their basic strength, which will lead to weaker bonding of the adsorbed species, thereby facilitating the desorption of the products from the surface of the catalysts to reduce coke deposition.

The recent study by Singh *et al.* revealed the reason for the variation in the Knoevenagel condensation reaction activity, as

shown in Fig. 14(b), due to the different surface amine sites after pretreatment of SBA-15-oxynitrides at different temperatures.<sup>147</sup> According to this study, they proposed a completely different mechanism of ammonia attack on siloxanes, as shown in Fig. 14(a), than that reported by Asefa *et al.*, enabling the production of secondary and even tertiary amines rather than just the production of primary amines.<sup>148</sup> Notably, the advanced characterization method employed, as shown in Fig. 14(c), directly confirmed the predominant presence of secondary amines on SBA-15-N900 and tertiary amines on SBA-15-N1200. Solid-state NMR and XPS studies, as shown in Fig. 14(d), demonstrated that the differences in the formation of surface primary, secondary, and tertiary amines led to variations in reactivity, with the activity dependent on the complex factors among the total amine content, the fraction of primary amine content, and the available surface area, while the concentration of the surface amine depended on the nitriding temperature. The presence of a high primary amine content is associated with high catalytic efficiency and a higher fraction of secondary/tertiary amines contributes to a decreased TON.<sup>147</sup>

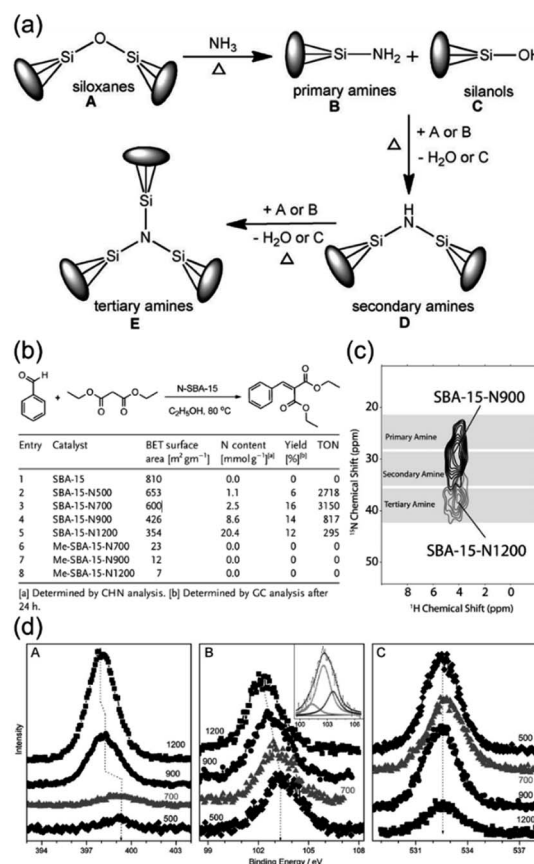


Fig. 14 (a) Mechanism of nitridation during ammonolysis. (b) Catalytic activity SBA-15-NT (SBA-15 was nitridated at T °C) for the Knoevenagel condensation reaction between benzaldehyde and diethyl malonate. (c) <sup>1</sup>H-detected <sup>15</sup>N-<sup>1</sup>H correlation spectrum obtained for SBA-15-N1200 (grey) and SBA-15-N900 (black). (d) XPS spectra for (A) N 1s, (B) Si 2p, and (C) O 1s core levels of various SBA-15-oxynitrides. Binding energy changes observed are indicated by a dotted line.<sup>147</sup> Reprinted with permission from ref. 147. Copyright © 2015, Wiley.



Research on bio-oil have gained significant attention in recent years due to the growing focus on environmental protection globally. Several base-catalyzed condensation reactions, such as esterification, aldol condensation and ketonization, are important intermediate steps in the production of second-generation biofuels by exploiting the intrinsic reactivity of bio-oil components. Numerous mild base catalysts have been identified to exhibit a stable performance in aldol condensation such as supported alkali or alkaline earth metals and other supported metal oxides. Recently, Puértolas *et al.* investigated the deoxygenation *via* aldol condensation for bio-oil by the use of mild base catalysts and illustrated the activity, selectivity and stability properties of supported MgO catalysts in the vapor phase condensation of propionaldehyde, while this performance was maximized upon the mechanochemical activation of a siliceous USY zeolite (Si/Al = 405) containing 1 wt% Mg(OH)<sub>2</sub>.<sup>149</sup> The IR studies on CO and CO<sub>2</sub> adsorption, CO<sub>2</sub>-TPD, XRD and STEM-mapping characterization combined with the variation in the reaction performance due to different amounts of MgO, as shown in Fig. 15(a and b), revealed that the moderation of the basic strength is facilitated by the high dispersion of small amounts of MgO on the siliceous USY zeolites prepared by mechanochemical activation, as shown in Fig. 15(c and d), which is ascribed to the incorporation of Mg<sup>2+</sup> in framework defects on the zeolite surface. The limited number of these defects leads to the formation of a undesirable MgO sub-phase with an increase in Mg content and fosters the non-selective conversion of propionaldehyde due to its strong basicity.<sup>149</sup>

**4.4.3 Performance in oil treatment applications.** Given that researchers have taken an interest in the use of solid base catalysts *via* refining processes, some programs for the production of low-carbon olefins such as FCC have received extensive attention in recent times.<sup>151</sup>

However, due to its carbonium ion mechanism which determines its susceptibility to hydrogen transfer, the possible carbon deposition on it can lead to a rapid decrease in catalyst activity or even rapid deactivation, and hence the high requirement for oil in the selection of the feedstock.<sup>152,153</sup> If heavier or inferior feedstock is used, given that it has a higher asphaltene content and other impurities, this will lead to more carbon deposition on the catalyst, while the pore structure of the ZSM-5 zeolite will limit the access of macromolecules to its active center, and the feedstock tends to accumulate gradually on the catalyst surface, eventually inactivating the catalyst.<sup>155</sup> Yoshimura *et al.* studied the effect of loading La<sub>2</sub>O<sub>3</sub> and P (*e.g.*, H<sub>3</sub>PO<sub>4</sub>) on ZSM-5 zeolite on the catalytic activity of naphtha cracking and the properties of these catalysts. It was shown that the La-loaded catalyst could inhibit the formation of BTX-like products, and thus promote the yields of ethylene and propylene to a certain extent. The loading of La and P did not affect the acidic properties of ZSM-5, while the inhibition of heavier products such as aromatics is due to the enhancement of the surface basicity by the introduction of La. Similar to the above-mentioned introduction of B<sub>2</sub>O<sub>3</sub> to stabilize the K loading, as mentioned in Section 3.3.3, the addition of P could stabilize Al in the zeolite framework, thereby enhancing the hydrothermal stability of the catalyst and stabilizing its catalytic activity.<sup>12</sup>

Due to the correlation between the catalytic cracking performance of zeolites and their acidic property and pore structure, researchers have attempted to optimize the coking problem in the treatment of heavy oils by modifying the zeolites with alkaline metals in recent years. Zhang *et al.* introduced alkali metal oxides into a bifunctional catalyst prepared by zeolite to crack vacuum residue oil, as shown in Table 4, and the results showed that while over-cracking and the dry gas yield in the reaction were improved to certain extent by the introduction of bases, the coke yield was not significantly reduced, and it can

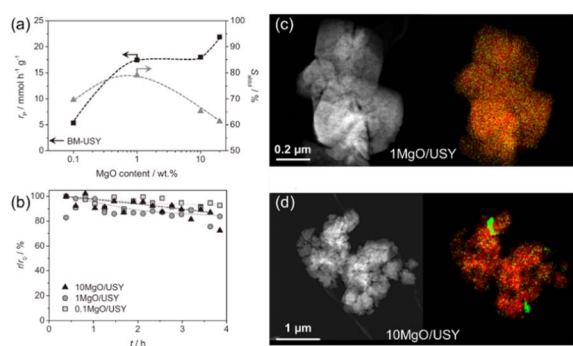


**Fig. 15** (a) Rate of propanal conversion (black) and selectivity to the aldol condensation products (grey) *versus* the MgO content over the MgO/USY zeolites. The arrow indicates the rate of propanal conversion over the BM-USY reference. Reaction conditions: 0.3 g, 400 °C, 6.25 kPa, He flow = 50 cm<sup>3</sup> min<sup>-1</sup>. (b) Relative decrease in the reaction rate observed in the vapor phase condensation of propanal over MgO/USY zeolites with different MgO contents. HAADF-STEM images (left) and elemental maps (right) of Si (red) and Mg (green) of the (c) 1 MgO/USY and (d) 10 MgO/USY zeolite catalysts. The scale bars apply to both images in the same row.<sup>149</sup> Reprinted with permission from ref. 149. Copyright © 2016, Elsevier.

**Table 4** Product distribution of VR cracking on hydrothermally treated catalysts.<sup>150</sup> Used with permission from ref. 150. Copyright © 2014, Elsevier

Test no.	1	2	3	4	5
Catalyst	FCC-800 <sup>a</sup>	BFC-800 <sup>b</sup>	BFC-850	BFC-800	BFC-850
Temp (°C)	503	500	499	499	497
Catalyst/oil ratio	6.3	6.3	6.3	4.2	4.2
Gas yield (wt%)	10.3	19.4	11.2	13.4	7.3
Liquid yield (wt%)	82.4	71.0	79.1	78.2	84.0
Coke yield (wt%)	7.3	9.6	9.7	8.4	8.7
Dry gas (vol%)	36.0	32.0	38.0	31.2	42.9
Conversion (%)	98.7	100.0	100.0	99.0	94.9

#### Distillation distribution of liquid

Gasoline (wt%)	38.5	58.4	43.8	55.4	29.8
Diesel (wt%)	42.3	38.0	43.9	33.3	34.7
VGO (wt%)	17.6	3.5	12.3	10.0	29.5
Heavy oil (wt%)	1.6	0.0	0.0	1.3	6.0

<sup>a</sup> FCC-T: FCC catalysts by hydrothermal treatment at T °C. <sup>b</sup> BFC-T: BFC catalysts (author's self-made bifunctional catalysts) by hydrothermal treatment at T °C.



be seen that the modification of zeolites by alkaline metals alone is not sufficient to solve the carbon deposition problem arising from the catalytic cracking of heavy oil.<sup>150</sup>

Recently, Wu *et al.* of CNOOC (China National Offshore Oil Corporation) developed DPC (direct petroleum cut to chemicals and materials) base-catalyzed technology for the catalytic cracking of heavy oil using base catalysts. All the base catalysts consisted of basic active components, additives, molding promoter, and carriers. Amorphous silicon oxide with a high specific surface area, silica-alumina composite oxide or SBA-15 carriers were selected to inhibit the adsorption of PAHs (polycyclic aromatic hydrocarbons) and non-hydrocarbon impurities. However, although these mesoporous structures could promote the macromolecular mass transfer in heavy oil, the heavy oil conversion and products yield such as LPG, gasoline and coke were all lower than acid catalysts. Tables 5 and 6 presents the natural properties of feedstock oil and the preparation information, reaction conditions and reaction results of this solid base, respectively.<sup>154,156</sup> Compared with delayed coking technology, as reported by the inventor, DPC technology with a base catalyst could reduce the formation of coke and promote the yield of LPG, C<sub>2</sub>–C<sub>4</sub>, light naphtha and heavy naphtha.<sup>157</sup>

## 5 Typical industrial applications

Acid catalysts have been well developed previously and many of them have been successfully utilized industrially in numerous industrial processes, such as naphtha cracking, isomerization, and alkylation. In contrast, the application of solid bases as catalysts came later than solid acids, and there were only a few examples of the successful application of solid bases as catalysts in the industry. One of the main reasons for this is that solid bases are sensitive to substances such as inherent moisture and carbon dioxide in the air. Meanwhile, the higher the strength of the base, the stronger the tendency to poisoning. Consequently, solid bases are difficult to prepare and store with stringent and demanding requirements, making it challenging to achieve convenient and inexpensive industrial applications.

Additionally, unlike most lab research, the importance in industrial applications is to control the nature, morphology, textural properties (surface area and porosity) and thermal, chemical and mechanical stability of solid base catalysts, and it is challenging to tackle these aspects in solid bases. The conventional synthesis process for industrial catalysts is as follows: chemicals (control impurities), catalyst precursor

Table 5 Natural properties of feedstock oil<sup>154</sup>

Item	Vacuum residue oil
Density, g cm <sup>-3</sup>	0.932
H–C ratio	1.75
Residual carbon, wt%	15.6
Basic nitride, ppm	1925.1
Acid value, mg KOH%	0.28
Element analysis, wt%	
	C
	H
	S
	N
Four components analysis, wt%	
	Saturated hydrocarbon, wt%
	Aromatic hydrocarbon, wt%
	Colloid, wt%
	Asphaltene, wt%

Table 6 Solid base composition and reaction results.<sup>154</sup>

Catalysts	Cat. 1	Cat. 2	Cat. 3
Carrier (wt%)	38% high specific surface area SiO <sub>2</sub>	37.81% alumina-silica mixed oxide-0.06%TiO <sub>2</sub> -0.13%Mn	37.81% SBA-15-0.06%TiO <sub>2</sub> -0.13%Mn
Alkaline earth metal (wt%)	8%MgO	8%CaO	8%CaO
Rare earth oxide (wt%)	—	1.5%CeO <sub>2</sub>	1.5%CeO <sub>2</sub>
Preparation condition	Slurry water content 73 wt%. Calcined at 550 °C for 4 h		
Aging condition	100% hydrothermal treatment at 800 °C for 17 h		
Reaction condition	Fluidized bed reactor, 0.2 MPa, 520 °C, steam/feed = 3 : 1(wt), ratio of catalyst to feed oil = 12, contact time = 2 s		
Feed	VR		
Dry gas (wt%)	1.58	1.04	2.23
LPG (wt%)	6.68	4.95	6.86
Gasoline (wt%)	13.59	16.53	17.42
Diesel (wt%)	15.27	16.12	15.7
Heavy oil (wt%)	48.21	53.68	51.83
Coke (wt%)	14.67	7.68	5.96





Table 7 Industrial processes in which solid base catalysts are used.<sup>16,154,157</sup>

Reaction	Catalyst	Year
<b>Alkylation</b>		
Alkylation of phenol with methanol	MgO	1970, 1985
Alkylation of xylene with butadiene	Na/K <sub>2</sub> CO <sub>3</sub>	1995
Alkylation of cumene with ethylene	Na/KOH/Al <sub>2</sub> O <sub>3</sub>	1988
<b>Isomerization</b>		
Isomerization of safrole to isosafrole	Na/NaOH/Al <sub>2</sub> O <sub>3</sub>	1988
Isomerization of 2,3-dimethyl-1-butene	Na/NaOH/Al <sub>2</sub> O <sub>3</sub>	1988
Isomerization of 3,5-vinylbicyclo [2,2,1] heptane	Na/NaOH/Al <sub>2</sub> O <sub>3</sub>	1988
Isomerization of 1,2-propadiene to propyne	K <sub>2</sub> O/Al <sub>2</sub> O <sub>3</sub>	1996
<b>Dehydration/condensation</b>		
Dehydration of 1-cyclohexylethanol	ZrO <sub>2</sub>	1986
Dehydration of propylamine-2-ol	ZrO <sub>2</sub> /KOH	1992
Isobutyraldehyde to diisopropyl ketone	ZrO <sub>2</sub>	1973
Dehydrotrimerization of isobutyraldehyde	BaO–CaO	1998
<b>Esterification</b>		
Esterification of ethylene oxide	Hydrotalcite	1994
Transesterification of triglycerides	ZnO–Al <sub>2</sub> O <sub>3</sub>	2006
<b>Catalytic cracking</b>		
Crude oil to chemicals	Alkali/alkaline earth metal oxide-highly mesoporous carrier	2022
<b>Miscellaneous</b>		
Carboxylic acids to aldehydes	ZrO <sub>2</sub> –Cr <sub>2</sub> O <sub>3</sub>	1988
Thiols from alcohols with hydrogen sulfide	Alkali/Al <sub>2</sub> O <sub>3</sub>	1988
Cyclization of imine with sulfur dioxide	Cs-zeolite	1995

(texture), form (texture, shape attrition resistance), and final catalyst (texture, attrition resistance).

However, due to the good catalytic properties of solid bases in some special base-catalyzed reactions (*e.g.*, isomerization of alkenes and alkynes, transesterification, Michael addition, condensation reactions and anti-Markovnikov hydroamination and hydroalkoxylation), only a few solid bases has been industrially applied to date. An industrial process for the production of chemicals by catalytic cracking of crude oil using a novel solid base catalyst has been added to the list, as shown in Table 7, which summarizes the solid base catalysts for industrial applications reported by Hideshi Hattori in 2015.<sup>8,16</sup> In recent years, the DPC catalyst was commercialized in the Huizhou refinery with an inventory of up to 26.5%, similar to an additive, given that the bottom cracking activity will be depressed with an increase in its proportion.<sup>8</sup> The mechanism of the proposed carbon anion has not been described and proven to date, but the lower yield of coke should be related to the inhibition of hydrogen transfer and aromatic condensation reactions due to the reduction in the number of acid sites. Thus, there are still too many unknowns in the field of oil cracking catalyzed by solid base catalysts, and thus more in-depth basic research and systematic analytical validation are needed.

It might be noteworthy that, as can be seen from Table 7, the solid base catalysts available for industrial applications currently exist mainly exclusively as metal oxides, whereas the catalytic activity of the zeolites named as basic-catalyst rarely reveals industrial or relevant applications in chemical processes

thus far. Indeed, the structure–activity relationship for the microporous basic properties of zeolites remains an open discussion. It is obvious that the zeolite acid–base pair is different from that of the homogeneous acid–base compounds and some solid metal oxides, given that their strength is influenced by the type of exchangeable cations, aluminum content, structural dimension, and porosity.<sup>158,159</sup>

Nevertheless, several reviews and articles published in the last decade indicated that solid bases are recognized as a type of environmentally friendly catalyst, and therefore research on solid base materials and their catalytic reactions showed an accelerated development in recent years despite their many challenges.

## 6 Conclusion and outlook

Alkali metals, alkaline earth metals, rare earth metals, and their oxides and compounds are now widely used in the preparation and development of base catalysts. Solid base catalysts, which are expected to be environmentally friendly, are gaining increasing attention from researchers and may provide new ideas to improve the reaction process and cope with environmental requirements and treatment of inferior heavy oil. However, to date, the corresponding research on solid base catalysts is still less than that on solid acids catalysts, the knowledge is more superficial, and the catalytic mechanisms in different types of reactions need further study and elaboration. The lack of systematic research on the catalytic mechanism of



bases is an important reason limiting the development of solid bases, and therefore the following are important:

(1) Establishing a systematic study of solid bases. The relationship between the number of active sites in solid bases and their strength and the reaction mechanism is still lacking in regular studies, and further studies on the reaction processes occurring at the active sites and their reaction mechanism will provide a more effective way for the preparation and application of solid base catalysts.

(2) Modelling and analysis of active sites through computer analogs and calculations. Different models of active sites on the surface of solid base catalysts are constructed, and the structure–activity relationships between the active sites and reaction performance are established through theoretical calculations and analysis, which can assist experimental studies in designing different catalyst configurations for application to specific reaction processes.

(3) Emphasis is placed on the development of basic research work such as high-end characterization. Given that there are electron cloud shifts and charge transfer in solid base catalytic processes, the description of microstructure can better explain the reaction mechanism and structure–activity relationships. The combination of electron cloud theory and characterization at the atomic level can provide theoretical support for the development of new solid base catalysts.

(4) When the reaction does not require a strong base, oxides and zeolites modified with alkali metal can be considered. The solid base with  $\text{Al}_2\text{O}_3$  as the carrier is stable in basicity and has good hydrothermal stability, and zeolites have good selectivity for the target products due to their intrinsic ability of selective shape and very high specific surface. Cs can be used to modify the oxides and zeolites when the reactions require superbases, but the cost of modification with Cs is high. Therefore, attention should be paid to the synthesis of solid base catalysts to improve the specific surface area and reduce the cost.

(5) Current studies have shown that solid base catalysts prepared with metal oxides can show a large change in basic strength, but their hydrothermal stability is poor and their specific surface area is low. Meanwhile, although solid base catalysts prepared with zeolites have a larger specific surface area and stronger hydrothermal stability, their basicity enhancement is limited. Therefore, the two components can be combined, which may achieve green conversion of inferior heavy oil, especially in the cracking process, where the fusion of the advantages of the two types of catalysts may be necessary.

## Conflicts of interest

There are no conflicts to declare.

## Acknowledgements

This work is financially supported by the National Key Research & Development Program of China (grant number 2022YFB3504000) and the Contract Projects of China Petroleum & Chemical Corporation (SINOPEC Corp.) [grant number 123031].

## Notes and references

- 1 S. Chen, F. Xiong and W. Huang, *Surf. Sci. Rep.*, 2019, **74**, 100471.
- 2 R. Lang, X. Du, Y. Huang, X. Jiang, Q. Zhang, Y. Guo, K. Liu, B. Qiao, A. Wang and T. Zhang, *Chem. Rev.*, 2020, **120**, 11986–12043.
- 3 Y. Ono and H. Hattori, *Solid Base Catalysis*, Springer Science & Business Media, Germany, 2012.
- 4 H. Hattori, *Chem. Rev.*, 1995, **95**, 537–558.
- 5 H. Pines and W. Haag, *J. Org. Chem.*, 1958, **23**, 328–329.
- 6 L. B. Sun, X. Q. Liu and H. C. Zhou, *Chem. Soc. Rev.*, 2015, **44**, 5092–5147.
- 7 Q. Wu, *Pet. Refin. Eng.*, 2022, **52**, 1–7.
- 8 A. X. He, L. G. Hou, F. Y. Jin, L. Xin and Q. Wu, *Pet. Refin. Eng.*, 2023, **53**, 34–38.
- 9 F. M. Alotaibi, S. González-Cortés, M. F. Alotibi, T. Xiao, H. Al-Megren, G. Yang and P. P. Edwards, *Catal. Today*, 2018, **317**, 86–98.
- 10 T. Wei, M. H. Wang, W. Wei, Y. H. Sun and B. Zhong, *Chemistry*, 2002, **65**, 594–600.
- 11 X. Z. Li and Q. Jiang, *Progress in catalysts for solid base, Low-carbon chemistry and chemical engineering*, 2005, vol. 30, pp. 42–48.
- 12 Y. Yoshimura, N. Kijima, T. Hayakawa, K. Murata, K. Suzuki, F. Mizukami, K. Matano, T. Konishi, T. Oikawa and M. Saito, *Catal. Surv. Asia*, 2001, **4**, 157–167.
- 13 M. S. Gao, G. H. Zhang, L. Zhao, J. S. Gao and C. M. Xu, *Ind. Eng. Chem. Res.*, 2023, **62**, 1215–1226.
- 14 M. A. Alabdullah, A. R. Gomez, J. Vittenet, A. Bendjeriou-Sedjerari, W. Xu, I. A. Abba and J. Gascon, *ACS Catal.*, 2020, **10**, 8131–8140.
- 15 N. Niwamanya, J. Zhang, C. Gao, D. T. Sekyere, A. Barigye, J. Nangendo and Y. Tian, *Fuel*, 2022, **328**, 125285.
- 16 H. Hattori, *Appl. Catal., A*, 2015, **504**, 103–109.
- 17 H. Pines, *Base-catalyzed Reactions of Hydrocarbons and Related Compounds*, Academic Press, New York, 2012.
- 18 H. Hattori, in *Studies in Surface Science and Catalysis*, Elsevier, 1993, vol. 78, pp. 35–49.
- 19 K. Tanabe, M. Misono, Y. Ono and H. Hattori, *New Solid Acids and Bases: Their Catalytic Properties*, Kodansha, Elsevier, Japan, 1989, ch. 2, p. 5.
- 20 M. Aziz, A. A. Jalil, S. Wongsakulphasatch and D. N. Vo, *Catal. Sci. Technol.*, 2020, **10**, 35–45.
- 21 M. Shirotori, S. Nishimura and K. Ebitani, *J. Mater. Chem. A*, 2017, **5**, 6947–6957.
- 22 T. C. Keller, K. Desai, S. Mitchell and J. Perez-Ramirez, *ACS Catal.*, 2015, **5**, 5388–5396.
- 23 K. Kajihara, N. Tezuka, M. Shoji, J. Wakasugi, H. Munakata and K. Kanamura, *Bull. Chem. Soc. Jpn.*, 2017, **90**, 1279–1286.
- 24 J. Dwyer and H. Schofield, *NATO ASI Ser., Ser. C*, 1994, **444**, 13–32.
- 25 K. Tanabe and W. F. Hölderich, *Appl. Catal., A*, 1999, **181**, 399–434.
- 26 J. C. Védrine, *Catalysts*, 2017, **7**, 341.



- 27 I. Fechete and J. C. Vedrine, *Nanotechnology in Catalysis: Applications in the Chemical Industry*, Energy Development, and Environment Protection, 2017, pp. 57–90.
- 28 H. Hattori, K. Maruyama and K. Tanabe, *J. Catal.*, 1976, **44**, 50–56.
- 29 M. Mohri, K. Tanabe and H. Hattori, *J. Catal.*, 1974, **32**, 144–147.
- 30 M. Bhagiyalakshmi, J. Y. Lee and H. T. Jang, *Int. J. Greenhouse Gas Control*, 2010, **4**, 51–56.
- 31 M. León, L. Faba, E. Díaz, S. Bennici, A. Vega, S. Ordonez and A. Auroux, *Appl. Catal., B*, 2014, **147**, 796–804.
- 32 K. Tanabe, M. Misono, Y. Ono and H. Hattori, in *New Solid Acids and Bases*, Elsevier, Oxford Amsterdam/New York/Tokyo, 1989, vol. 51.
- 33 M. Anpo, G. Costentin, E. Giamello, H. Lauron-Pernot and Z. Sojka, *J. Catal.*, 2021, **393**, 259–280.
- 34 X. Wang and J. D. Lee, *Modell. Simul. Mater. Sci. Eng.*, 2010, **18**, 85010.
- 35 S. Arndt, G. Laugel, S. Levchenko, R. Horn, M. Baerns, M. Scheffler, R. Schlögl and R. Schomäcker, *Catal. Rev.: Sci. Eng.*, 2011, **53**, 424–514.
- 36 C. Chizallet, G. Costentin, H. Lauron-Pernot, J. M. Krafft, M. Che, F. O. Delbecq and P. Sautet, *J. Phys. Chem. C*, 2008, **112**, 16629–16637.
- 37 S. Coluccia and A. J. Tench, *Stud. Surf. Sci. Catal.*, 1981, **7**, 1154–1169.
- 38 M. Che and A. J. Tench, in *Advances in Catalysis*, Elsevier, 1982, vol. 31, pp. 77–133.
- 39 H. Hattori, *J. Jpn. Pet. Inst.*, 2004, **47**, 67–81.
- 40 D. Cornu, H. Petitjean, G. Costentin, H. Guesmi, J. Krafft and H. Lauron-Pernot, *Phys. Chem. Chem. Phys.*, 2013, **15**, 19870–19878.
- 41 G. A. Mutch, S. Shulda, A. J. McCue, M. J. Menart, C. V. Ciobanu, C. Ngo, J. A. Anderson, R. M. Richards and D. Vega-Maza, *J. Am. Chem. Soc.*, 2018, **140**, 4736–4742.
- 42 C. H. Xue, R. J. Wang and J. Y. Zhang, *Acta Pet. Sin.*, 2002, 30–35.
- 43 G. Zhang, H. Hattori and K. Tanabe, *Bull. Chem. Soc. Jpn.*, 1989, **62**, 2070–2072.
- 44 M. Bailly, C. Chizallet, G. Costentin, J. Krafft, H. Lauron-Pernot and M. Che, *J. Catal.*, 2005, **235**, 413–422.
- 45 H. Petitjean, H. Guesmi, H. Lauron-Pernot, G. Costentin, D. Loffreda, P. Sautet and F. Delbecq, *ACS Catal.*, 2014, **4**, 4004–4014.
- 46 K. Akutu, H. Kabashima, T. Seki and H. Hattori, *Appl. Catal., A*, 2003, **247**, 65–74.
- 47 H. Hattori, *Appl. Catal., A*, 2001, **222**, 247–259.
- 48 Y. Fukuda, H. Hattori and K. Tanabe, *Bull. Chem. Soc. Jpn.*, 1978, **51**, 3150–3153.
- 49 Y. Imizu, K. Sato and H. Hattori, *J. Catal.*, 1982, **76**, 65–74.
- 50 M. Utiyama, H. Hattori and K. Tanabe, *J. Catal.*, 1978, **53**, 237–242.
- 51 S. C. Shen, X. Chen and S. Kawi, *Langmuir*, 2004, **20**, 9130–9137.
- 52 A. J. Lundeen and R. Vanhoozer, *J. Org. Chem.*, 1967, **32**, 3386–3389.
- 53 T. Tomatsu, N. Yoneda and H. Ohtsuka, *J. Jpn. Oil Chem. Soc.*, 1968, **17**, 236–245.
- 54 K. M. Minachev, Y. S. Khodakov and V. S. Nakhshunov, *J. Catal.*, 1977, **49**, 207–215.
- 55 H. Noller, J. A. Lercher and H. Vinek, *Mater. Chem. Phys.*, 1988, **18**, 577–593.
- 56 W. Ueda, T. Yokoyama, Y. Moro-Oka and T. Ikawa, *Chem. Lett.*, 1985, **14**, 1059–1062.
- 57 H. Matsushashi, M. Oikawa and K. Arata, *Langmuir*, 2000, **16**, 8201–8205.
- 58 S. Jayashree and M. Ashokkumar, *Catalysts*, 2018, **8**, 601.
- 59 J. Jupille and G. Thornton, *Defects at Oxide Surfaces*, Springer, 2015.
- 60 D. He, D. Chen, H. Hao, J. Yu, J. Liu, J. Lu, F. Liu, G. Wan, S. He and Y. Luo, *Appl. Surf. Sci.*, 2016, **390**, 959–967.
- 61 T. Rajesh and R. N. Devi, *J. Phys. Chem. C*, 2014, **118**, 20867–20874.
- 62 Z. Zhang, Y. Wang, J. Lu, J. Zhang, M. Li, X. Liu and F. Wang, *ACS Catal.*, 2018, **8**, 2635–2644.
- 63 K. Yu, L. L. Lou, S. Liu and W. Zhou, *Adv. Sci.*, 2020, **7**, 1901970.
- 64 K. Yu, D. Lei, Y. Feng, H. Yu, Y. Chang, Y. Wang, Y. Liu, G. Wang, L. Lou and S. Liu, *J. Catal.*, 2018, **365**, 292–302.
- 65 L. Qi, Q. Yu, Y. Dai, C. Tang, L. Liu, H. Zhang, F. Gao, L. Dong and Y. Chen, *Appl. Catal., B*, 2012, **119**, 308–320.
- 66 L. Nie, D. Mei, H. Xiong, B. Peng, Z. Ren, X. I. P. Hernandez, A. DeLaRiva, M. Wang, M. H. Engelhard and L. Kovarik, *Science*, 2017, **358**, 1419–1423.
- 67 J. Shan, F. R. Lucci, J. Liu, M. El-Soda, M. D. Marcinkowski, L. F. Allard, E. C. H. Sykes and M. Flytzani-Stephanopoulos, *Surf. Sci.*, 2016, **650**, 121–129.
- 68 K. Otake, Y. Cui, C. T. Buru, Z. Li, J. T. Hupp and O. K. Farha, *J. Am. Chem. Soc.*, 2018, **140**, 8652–8656.
- 69 J. Xie, K. Yin, A. Serov, K. Artyushkova, H. N. Pham, X. Sang, R. R. Unocic, P. Atanassov, A. K. Datye and R. J. Davis, *ChemSusChem*, 2017, **10**, 359–362.
- 70 C. Wang, G. Garbarino, L. F. Allard, F. Wilson, G. Busca and M. Flytzani-Stephanopoulos, *ACS Catal.*, 2016, **6**, 210–218.
- 71 J. Cho, D. Kwon, I. Yang, S. An and J. C. Jung, *Mol. Catal.*, 2021, **510**, 111677.
- 72 S. Hu, W. Wang, M. Yue, G. Wang, W. Gao, R. Cong and T. Yang, *ACS Appl. Mater. Interfaces*, 2018, **10**(18), 15895–15904.
- 73 Y. Yang, D. Wang, P. Jiang, W. Gao, R. Cong and T. Yang, *Mol. Catal.*, 2020, **490**, 110914.
- 74 G. Pomalaza, P. A. Ponton, M. Capron and F. Dumeignil, *Catal. Sci. Technol.*, 2020, **10**, 4860–4911.
- 75 T. Yokoyama, T. Setoyama, N. Fujita, M. Nakajima, T. Maki and K. Fujii, *Appl. Catal., A*, 1992, **88**, 149–161.
- 76 J. Wang, W. Yang, C. Wu, Y. Gong, J. Zhang and C. Shen, *ACS Sustain. Chem. Eng.*, 2020, **8**, 16960–16967.
- 77 K. Tanabe, H. Hattori, T. Sumiyoshi, K. Tamaru and T. Kondo, *J. Catal.*, 1978, **53**, 1–8.
- 78 J. H. Kolts and G. A. Delzer, *Science*, 1986, **232**, 744–746.
- 79 K. K. Pant and D. Kunzru, *Chem. Eng. J.*, 2002, **87**, 219–225.
- 80 K. K. Pant and D. Kunzru, *Can. J. Chem. Eng.*, 1999, **77**, 150–155.





- 81 S. M. Jeong, J. H. Chae, J. Kang, S. H. Lee and W. Lee, *Catal. Today*, 2002, **74**, 257–264.
- 82 A. A. Lemonidou and I. A. Vasalos, *Appl. Catal.*, 1989, **54**, 119–138.
- 83 M. L. Kaliya and S. B. Kogan, *Catal. Today*, 2005, **106**, 95–98.
- 84 K. Narasimharao and F. S. Al-Sultan, *Fuel*, 2020, **280**, 118599.
- 85 C. Boyadjian, L. Lefferts and K. Seshan, *Appl. Catal., A*, 2010, **372**, 167–174.
- 86 M. Nagao, H. Hamano, K. Hirata, R. Kumashiro and Y. Kuroda, *Langmuir*, 2003, **19**, 9201–9209.
- 87 J. Sá, M. Ace, J. J. Delgado, A. Goguet, C. Hardacre and K. Morgan, *ChemCatChem*, 2011, **3**, 394–398.
- 88 F. Cavani, N. Ballarini and A. Cericola, *Catal. Today*, 2007, **127**, 113–131.
- 89 S. M. Jeong, J. H. Chae and W. H. Lee, *Ind. Eng. Chem. Res.*, 2001, **40**, 6081–6086.
- 90 P. Lhonore, J. Quibel and M. Senes, *US Pat.*, 3624176A, 1971.
- 91 A. A. Lemonidou, I. A. Vasalos, E. J. Hirschberg and R. J. Bertolacini, *Ind. Eng. Chem. Res.*, 1989, **28**, 524–530.
- 92 B. Basu and D. Kunzru, *Ind. Eng. Chem. Res.*, 1992, **31**, 146–155.
- 93 R. Mukhopadhyay and D. Kunzru, *Ind. Eng. Chem. Res.*, 1993, **32**, 1914–1920.
- 94 V. A. Kumar, K. K. Pant and D. Kunzru, *Appl. Catal., A*, 1997, **162**, 193–200.
- 95 T. Tomita, K. Kikuchi and T. Sakamoto, *US Pat.*, 3767567A, 1973.
- 96 Y. Y. Tian, Y. J. Che, M. S. Chen, W. Feng, J. H. Zhang and Y. Y. Qiao, *Energy Fuels*, 2019, **33**, 7297–7304.
- 97 R. Y. Tang, Y. Y. Tian, Y. Y. Qiao, G. M. Zhao and H. F. Zhou, *Energy Fuels*, 2016, **30**, 8855–8862.
- 98 R. Y. Tang, Y. Y. Tian, J. L. Cai and Y. Y. Qiao, *Chem. Eng. Oil Gas*, 2015, **44**, 23–27.
- 99 R. Y. Tang, M. Yuan, K. Liu, H. F. Li, J. T. Zhang and Y. Y. Tian, *J. Energy Inst.*, 2019, **92**, 1936–1943.
- 100 Y. Okamoto, M. Ogawa, A. Maezawa and T. Imanaka, *J. Catal.*, 1988, **112**, 427–436.
- 101 J. Weitkamp, M. Hunger and U. Ryma, *Microporous Mesoporous Mater.*, 2001, **48**, 255–270.
- 102 R. J. Davis, *J. Catal.*, 2003, **216**, 396–405.
- 103 D. Barthomeuf, *J. Phys. Chem.*, 1984, **88**, 42–45.
- 104 D. Barthomeuf, G. Coudurier and J. C. Vedrine, *Mater. Chem. Phys.*, 1988, **18**, 553–575.
- 105 R. T. Sanderson, *J. Am. Chem. Soc.*, 1983, **105**, 2259–2261.
- 106 W. Gruenert, M. Muhler, K. Schroeder, J. Sauer and R. Schloegl, *J. Phys. Chem.*, 1994, **98**, 10920–10929.
- 107 M. Sánchez-Sánchez and T. Blasco, *J. Am. Chem. Soc.*, 2002, **124**, 3443–3456.
- 108 T. Yashima, K. Sato, T. Hayasaka and N. Hara, *J. Catal.*, 1972, **26**, 303–312.
- 109 A. Corma and R. M. Martin-Aranda, *J. Catal.*, 1991, **130**, 130–137.
- 110 T. Yashima, H. Suzuki and N. Hara, *J. Catal.*, 1974, **33**, 486–492.
- 111 A. Philippou, J. Rocha and M. W. Anderson, *Catal. Lett.*, 1999, **57**, 151–153.
- 112 J. Shabtai, R. Lazar and E. Biron, *J. Mol. Catal.*, 1984, **27**, 35–43.
- 113 A. Corma, V. Fornes, R. M. Martin-Aranda, H. Garcia and J. Primo, *Appl. Catal.*, 1990, **59**, 237–248.
- 114 D. Barthomeuf, in *Studies in Surface Science and Catalysis*, Elsevier, 1997, vol. 105, pp. 1677–1706.
- 115 A. Corma, R. M. Martin-Aranda and F. Sanchez, *J. Catal.*, 1990, **126**, 192–198.
- 116 L. R. Martens, P. J. Grobet and P. A. Jacobs, *Nature*, 1985, **315**, 568–570.
- 117 P. J. Grobet, L. Martens, W. Vermeiren, D. Huybrechts and P. A. Jacobs, in *Small Particles and Inorganic Clusters*, Springer, 1989, pp. 37–40.
- 118 S. V. Bordawekar and R. J. Davis, *J. Catal.*, 2000, **189**, 79–90.
- 119 E. J. Dskocil and P. J. Mankidy, *Appl. Catal., A*, 2003, **252**, 119–132.
- 120 E. J. Dskocil and R. J. Davis, *J. Catal.*, 1999, **188**, 353–364.
- 121 U. Meyer, H. Gorzawski and W. F. Hölderich, *Catal. Lett.*, 1999, **59**, 201–206.
- 122 F. Yagi and H. Hattori, *Microporous Mater.*, 1997, **9**, 247–251.
- 123 L. Martens, W. Vermeiren, P. J. Grobet and P. A. Jacobs, in *Studies in Surface Science and Catalysis*, Elsevier, 1987, vol. 31, pp. 531–542.
- 124 J. C. Kim, H. Li, C. Chen and M. E. Davis, *Microporous Mater.*, 1994, **2**, 413–423.
- 125 F. Yagi, N. Kanuka, H. Tsuji, S. Nakata, H. Kita and H. Hattori, *Microporous Mater.*, 1997, **9**, 229–235.
- 126 M. Hunger, U. Schenk and J. Weitkamp, *J. Mol. Catal. A: Chem.*, 1998, **134**, 97–109.
- 127 F. Yagi, H. Tsuji and H. Hattori, *Microporous Mater.*, 1997, **9**, 237–245.
- 128 J. Li and R. J. Davis, *Appl. Catal., A*, 2003, **239**, 59–70.
- 129 J. H. Zhu, Y. Chun, Y. Wang and Q. H. Xu, *Catal. Today*, 1999, **51**, 103–111.
- 130 C. B. Dartt and M. E. Davis, *Catal. Today*, 1994, **19**, 151–186.
- 131 S. Ernst, T. Bongers, C. Casel and S. Munsch, in *Studies in Surface Science and Catalysis*, Elsevier, 1999, vol. 125, pp. 367–374.
- 132 K. R. Kloetstra and H. Van Bekkum, in *Studies in Surface Science and Catalysis*, Elsevier, 1997, vol. 105, pp. 431–438.
- 133 M. Ziolek, A. Michalska, J. Kujawa and A. Lewandowska, *Nanoporous Materials III: Proceedings of the 3rd International Symposium on Nanoporous Materials*, Elsevier Science Limited, Ottawa, Ontario, Canada, 2002, vol. 141, pp. 411.
- 134 R. M. Dessau, *Zeolites*, 1990, **10**, 205–206.
- 135 K. Tanabe, *Solid Acids and Bases: Their Catalytic Properties*, Academic Press, New York and London, Kodansha, 1970.
- 136 J. H. Zhu, Y. Wang and Y. Tsutomu, *Chin. J. Catal.*, 1996, **17**, 286–290.
- 137 J. H. Zhu, Y. Chun, Y. Wang and M. Tu, *Chin. Sci. Bull.*, 1997, **42**, 1118–1119.
- 138 J. H. Zhu, Y. Chun, Y. Wang and Q. H. Xu, *Chin. Sci. Bull.*, 1999, **44**, 897–902.



- 139 J. H. Zhu, H. Tsuji, H. Kabashima, H. Hattori and H. Kita, *Chin. Chem. Lett.*, 1995, **6**, 811–814.
- 140 J. H. Zhu, Y. Chun, Y. Qin and Q. Xu, *Microporous Mesoporous Mater.*, 1998, **24**, 19–28.
- 141 Y. Chun, J. H. Zhu and Q. H. Xu, *Chin. J. Catal.*, 1997, **18**, 298–301.
- 142 J. H. Zhu, Y. Wang, Y. Chun and X. S. Wang, *J. Chem. Soc., Faraday Trans.*, 1998, **94**, 1163–1169.
- 143 T. Yamaguchi, J. Zhu, Y. Wang, M. Komatsu and M. Ookawa, *Chem. Lett.*, 1997, **26**, 989–990.
- 144 J. H. Zhu and Y. Wang, *Chin. J. Catal.*, 1997, **18**, 498–502.
- 145 Y. Chun, J. H. Zhu, Y. Wang and Q. H. Xu, *Chin. Sci. Bull.*, 1998, **43**, 721–724.
- 146 J. H. Zhu, Y. Chun, Y. Wang and Q. H. Xu, *Mater. Lett.*, 1997, **33**, 207–210.
- 147 B. Singh, K. R. Mote, C. S. Gopinath, P. K. Madhu and V. Polshettiwar, *Angew. Chem., Int. Ed.*, 2015, **54**, 5985–5989.
- 148 T. Asefa, M. Kruk, N. Coombs, H. Grondy, M. J. MacLachlan, M. Jaroniec and G. A. Ozin, *J. Am. Chem. Soc.*, 2003, **125**, 11662–11673.
- 149 B. A. Puértolas, T. C. Keller, S. Mitchell and J. Pérez-Ramírez, *Appl. Catal., B*, 2016, **184**, 77–86.
- 150 Y. M. Zhang, D. P. Yu, W. L. Li, S. Q. Gao and G. W. Xu, *Fuel*, 2014, **117**, 1196–1203.
- 151 A. Corma, E. Corresa, Y. Mathieu, L. Sauvanaud, S. Al-Bogami, M. S. Al-Ghrami and A. Bourane, *Catal. Sci. Technol.*, 2017, **7**, 12–46.
- 152 R. Pujro, M. Falco and U. Sedran, *J. Chem. Technol. Biotechnol.*, 2016, **91**, 336–345.
- 153 R. B. Wang, *Acta Pet. Sin.*, 2021, **37**, 384–390.
- 154 Q. Wu, B. Li, C. L. Guo, J. Z. Zang, Z. H. Sun, M. Y. He, J. X. Fan, J. Guo, F. Y. Jin and Y. P. Gong, CN Pat., 113509925A, 2021.
- 155 N. Rahimi and R. Karimzadeh, *Appl. Catal., A*, 2011, **398**, 1–17.
- 156 Q. Wu, J. Z. Zang, B. Li, J. X. Fan, Z. H. Sun, Y. Zhao, J. Guo, W. Zhou, Y. P. Gong and L. W. Hou, CN Pat., 113477247A, 2021.
- 157 Q. Wu, *Fuel*, 2023, **332**, 126132.
- 158 G. Busca, *Microporous Mesoporous Mater.*, 2017, **254**, 3–16.
- 159 V. Verdoliva, M. Saviano and S. De Luca, *Catalysts*, 2019, **9**, 248.

